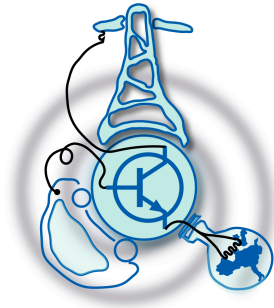# Steady and Dynamic Electrical Study for a Floating Photovoltaic Plant

by

Pablo Palacio Sánchez

Submitted to the Department of Electrical Engineering, Electronics,
Computers and Systems
in partial fulfillment of the requirements for the degree of
Master Course in Electrical Energy Conversion and Power Systems
at the
UNIVERSIDAD DE OVIEDO
June 2019

Author . . . .

Certified by . . . .
Vicente Garófalo
Company Coordinator
Thesis Supervisor

Certified by . . . .
Cristina González Morán
Associate Professor
Thesis Supervisor

Steady and Dynamic Electrical Study for a Floating Photovoltaic Plant

by

Pablo Palacio Sánchez

Submitted to the Department of Electrical Engineering, Electronics, Computers and Systems
on June 21, 2019, in partial fulfillment of the
requirements for the degree of
Master Course in Electrical Energy Conversion and Power Systems

Abstract

Large-scale solar photovoltaic (PV) power plants are consolidated as an alternative to conventional energy sources. However, these plants require large land areas which can be a challenge for those land-limited regions such as islands or countries with high population densities. Another issue of high capacity PV plants is to deal with elevated operating temperatures that negatively affect to the modules efficiency.

Therefore, to overcome these issues, installing PV modules over unused water surfaces has become a feasible option. These floating photovoltaic plants or commonly named "*floatovoltaics*" are currently a trend in Asian countries, whose installed capacity is continuously increasing. Floating solar energy possesses important advantages as an increase in the energy yield due to lower operating temperatures, reducing power losses or water quality improvement.

The objective of this Master Thesis (MTh) is to analyze the electrical performance of a 50 MW floating photovoltaic (FPV) power plant. It will be sited over a hydropower reservoir in Spain, in order to evaluate its grid-connection impact into the Spanish electrical network. The assessment will consist on carrying out steady and dynamic studies of the plant to check the compliance of the operating conditions established in the Spanish network code.

Out of these studies, it is concluded that the proposed FPV plant results in full compliance with the network connection requirements.

Keywords - Renewable energy, floating solar energy, grid code, PowerFactory

Thesis Supervisor: Vicente Garófalo
Title: Company Coordinator

Thesis Supervisor: Cristina González Morán
Title: Associate Professor

Acknowledgments

After four years as a bachelor student and two years as a master's one, I will conclude my stage at University of Oviedo with the presentation of this Master Thesis. The last two years, have been very productive but also quite tough and stressful. Nonetheless, I have grown up and developed new skills and abilities that will help me not only in my professional life, but also socially. For this reason, I would like to thank all the professors that were involved in the master's degree.

First of all, I would like to be grateful to my parents and my brother, who where the main support throughout all these years, supporting me every day, getting that I would not give up and for their unconditional support and efforts made during my internship in Pamplona.

Special acknowledge to my girlfriend for her love, support and for all the time I have taken her away.

At last, thanks to all the people that have shared moments during this period, in special my classmates Nacho, Andrés, Tania, Alejandro and Francisco.

Contents

List of Figures

List of Tables

Chapter 1

Introduction

1.1 Thesis Motivation

The development of renewable energies still has a lot of room for improvement. In the last years, photovoltaic generation costs have been reduced significantly, while greater modules effectiveness have been achieved. These motivate for a future scenario, with a massive penetration of renewable energies towards a future decarbonised power system. However, the design of large-scale PV power plants present several challenges: land availability and acquisition, complex civil and geo-technical studies or the plant site [1], [2] are some of them.

Therefore, to overcome these issues, a new technology has emerged: floating solar photovoltaic (FPV) plants or "*floatovoltaics*". It consists on placing the solar modules over floating platforms in unused water surfaces such as irrigation canals, water ponds or reservoirs. An example of a small FPV plant, located in Japan is presented in figure 1-1.

Currently, floating solar photovoltaic plants have been developed mainly in Asian countries (China, Japan, Indonesia and Taiwan), but other small-scale plants has been tested in France, United Kingdom, Norway and Portugal[1].

Figure 1-1: Kawarayama IKE - 1,428 kWp floating solar plant in Japan [3]

Thus, *floatovoltaics* could be an important opportunity for Spain to become the European leader in renewable energies. Factors aiming this event are the expected national energy transition, with significant investments, not only in renewable power plants but also, in energy storage or sustainable transportation. On February 22nd 2019, the Spanish Government presented the foundations to accomplish this energy transition in the *Energy and Climate Integrated National Plan (PNIEC)* [4].

By analyzing the PNIEC report, the expected power capacity increase by year 2030 is of 53 GW, from which 32.1 GW are destined to photovoltaic energy. This opens a new scenario for the PV energy market, which currently only counts with 4.7 GW installed. Additionally, since Spain has several hydropower facilities and water reservoirs, floating solar photovoltaics seems to be a technical alternative to achieve the energy transition objectives.

1.2 Description of a floating solar photovoltaic plant

The design and operation of a floating photovoltaic (FPV) plant and the one of a land-based PV plant are very similar. The main difference relies on the electrical

equipment, which is installed on floating platforms [1], [5]. A general layout of a FPV plant is represented in figure 1-2.
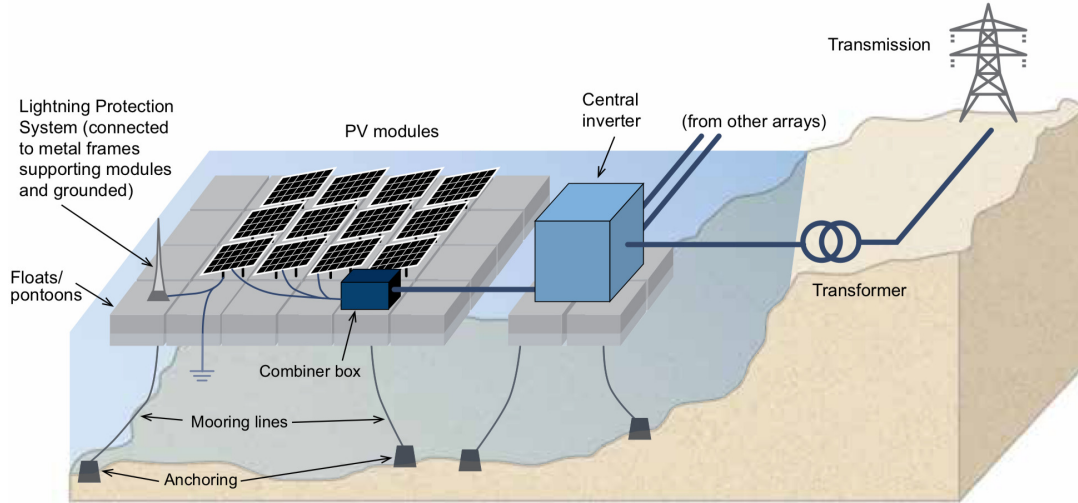
Figure 1-2: General layout configuration for a floating PV plant [1]

The PV modules generate electricity in direct current (DC) and all the energy from the arrays is collected at the combiner boxes. They are connected to central or string inverters [5] [1] to convert the current into AC. For this thesis, central inverter configuration is used, following an arrangement similar to the one exposed in figure 1-3a.

However, the most critical components in a FPV plant are the floating platforms, mooring lines and the anchoring system, being the main elements that rises the overall investment costs. In the majority of large-scale FPV plants, the common floating platforms used are the pure float floating system shown in figure 1-4a [1] or the pontoon-type float presented in figure 1-4b. The anchoring of the platform generally depends of the conditions where the plant is going to be installed: water profile, depth, land conditions and water level variations.

---

[1]Central inverters are generally used for large scale plants, whereas string inverters are used for lower capacities. The difference between these two inverter configurations is represented in figure 1-3. This tendency is currently changing because of inverter costs.
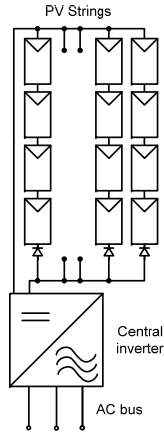
(a) Central inverter
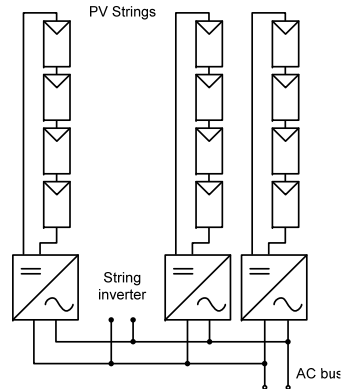
(b) String inverter

Figure 1-3: Inverter's configuration in a large-scale FPV plant: a) Central inverter, b) String inverter

(a) Pure float floating system [1]

(b) Pontoon type floating system [6]

Figure 1-4: Main floating structures used in FPV plants: a) pure float, b) pontoon structure

1.2.1 Situation of floating photovoltaics in the global market

Floatovoltaics came up for the first time in 2007, with a small pilot project in Japan. After that, several countries such as France, UK, United States or China followed this new technology with small testing systems. But it was not until 2013 when floating PV plants up to 1 MWp started to be deployed in countries such as Japan, Korea, Indonesia, Taiwan and China [1]. Some European countries have also tested it with small-scale plants in UK, Netherlands or Portugal, in which EDP became the first utility to install *floatovoltaics* combined with a hydropower plant.

Currently, with the reduction of generation costs and modules efficiency's increase, capacity of FPV plants have reached more than several tens of megawatts. China has become the world leader in this technology, installing plants with more than 100 MWp in 2018 [1], [7]. Countries of Southeast Asia (Taiwan, Viet Nam and Indonesia) are also planning to install several GWs of floating photovoltaics in future years.
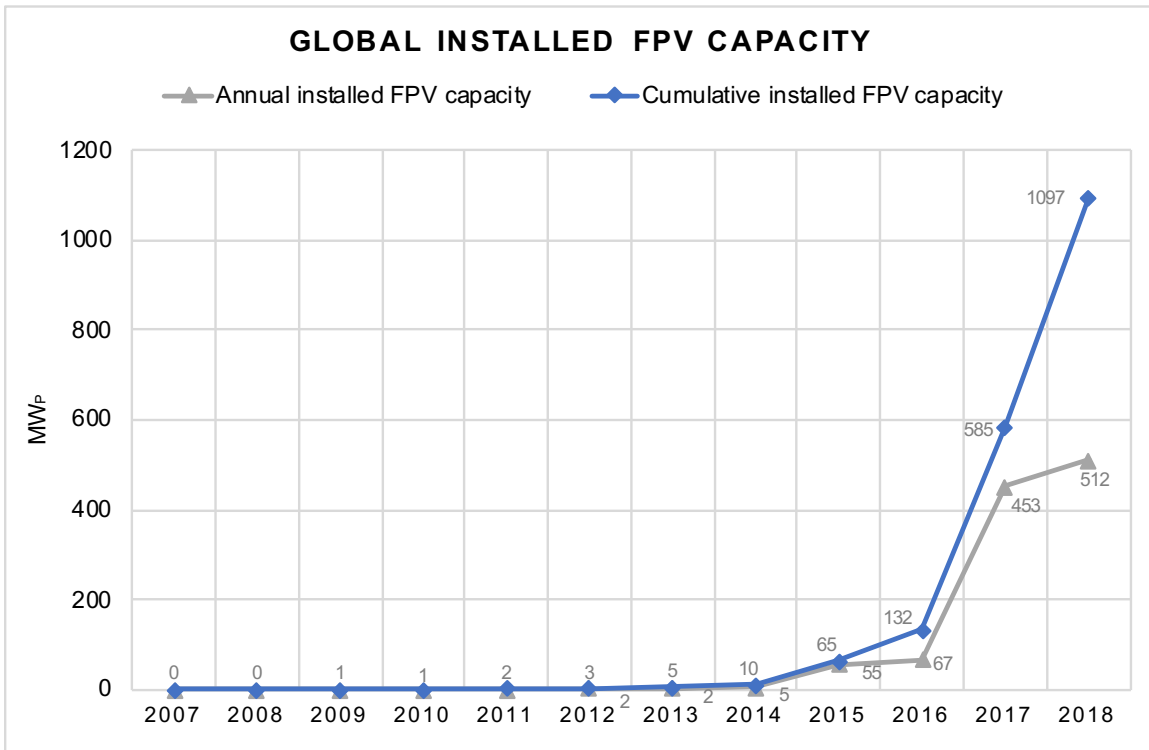
Figure 1-5: Evolution of global installed floating solar photovoltaic capacity

In figure 1-5, it can be observed the evolution of the FPV capacity installed since 2007. As it was commented, *floatovoltaics* several research projects were developed in 2013. However, it is in 2016 when the technology breaks with the economic barriers, becoming an energy generation alternative. During the last two years, FPV capacity increased 453 and 512 MWp respectively, reaching a global installed capacity over 1 GWp. This upward trend indicates that floating solar energy is being consolidated in the global energy market, increasing the opportunities for a higher penetration of renewable energies into electrical grids.

1.3   Potential advantages of floatovoltaics

The energy performance of floating solar modules have been analyzed in several projects since 2007. Results from several projects as [8], [9], conclude that the energy performance is improved. As explained by Wysocki in [11], this is due to the cooling effect of the water, which contributes to decreasing the operating cell temperature.

Wasynczuk analyzed in [12] the dynamic behaviour of a small-scale PV system against different ambient conditions. In figure 1-6a, the I-V curve of the PV array is characterized by Wasynczuk, where it is determined that the maximum power for each condition takes place at the lower temperature (T $= 28°C$). Generally, these electrical characteristics are given by the manufacturers in their solar module's datasheet. As example, figure 1-6b represents the temperature cell dependence of a solar module from the manufacturer *Jinko Solar*. The green curve represents the maximum output power generated by the cell. As long as the cell temperature is reduced, the voltage increase rate is greater than the current decrease one. As consequence, the output power is higher for lower temperatures.

In 2016, the Portuguese utility EDP, developed a pilot project where they combined a 220 kW floating photovoltaic installation with an existent hydropower plant. According to their results, the efficiency of the modules was measured to be 10%
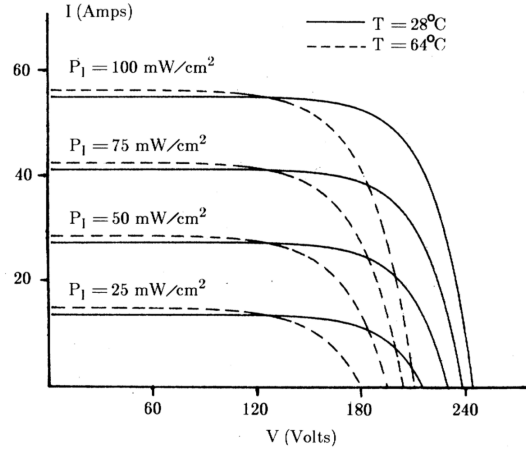
(a) I-V characteristic curve for a PV array
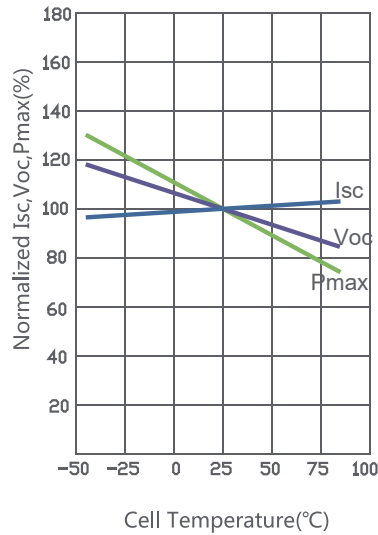
(b) Temperature dependence of I_{sc}, V_{oc}, P_{max} [10]

Figure 1-6: Solar cell power dependence on ambient conditions: a) PV array I-V characteristic curve, b) Cell temperature dependence

higher compared to a ground-mounted PV system, achieving higher energy yields than expected [13]. Additionally, other potential advantages of floating solar involve:

- Water quality is improved, since algae growth is decreased due to the platform's shadow [14]

- The shadow generated by the platform, also reduces evaporation, contributing to keep water levels [15]

- In case of adding floatovoltaics to hydropower plants, they can use the existent

electrical infrastructure

- The hybridization with pumped-storage hydropower plants set up a massive energy storage technology [9]

On the other hand, still there are important drawbacks regarding to this technology. The capital costs of FPV are higher compared to land-based PV plants because of the need of floating platforms, moorings and marine electrical components [1], [5], [16]. Nevertheless, it is expected that installation costs will drop in coming years due to economies of scale. Another issue is the lack of specific regulations regarding to water treatment licenses and environmental impacts.

1.4 Objectives

Once the topic of this project has been presented, the objective of the thesis is to analyze the grid interconnection impact of a 50 MW floating photovoltaic plant. The FPV plant will be located over the Almendra's reservoir, located in Salamanca, Spain. An aerial view of the geographic site of the plant is included in figure 1-7.
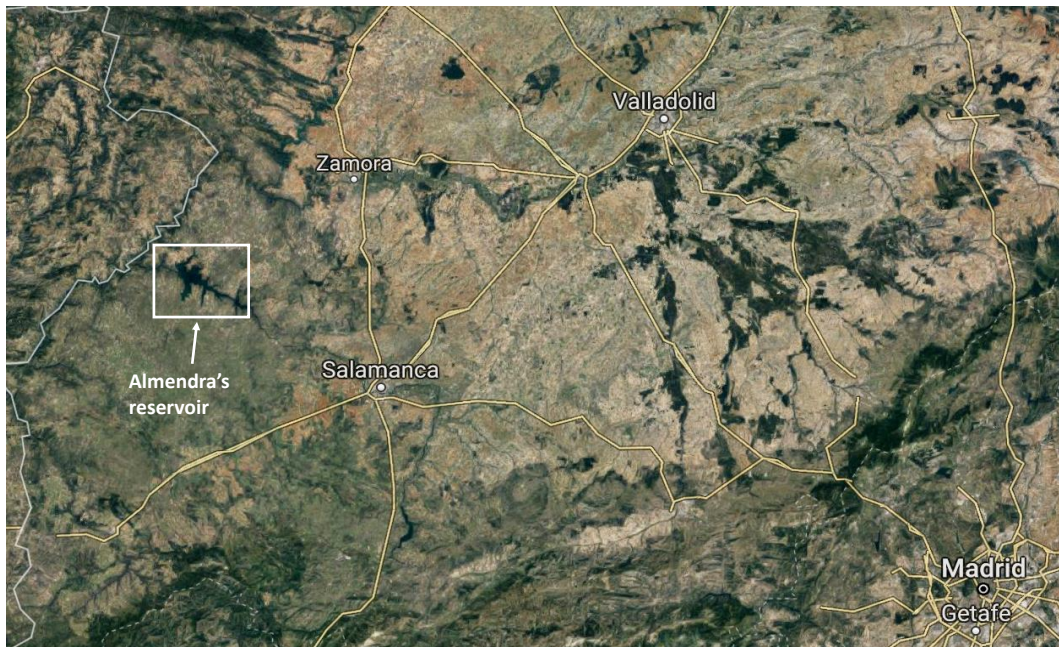
Figure 1-7: Geographical aerial view of the FPV plant's location

The choice of this location is due to the fact that it is one of the largest reservoirs in Spain, where the Villarino's hydropower plant is installed. This hydropower plant is the third biggest one, with a capacity of 857 MWp [17]. In addition, the surroundings are a non-mountainous area, being appropriate for a photovoltaic plant.

Therefore, the main purpose of this master thesis is to study if the FPV plant is able to comply with the network connection and operating requirements established by the Spanish transmission grid operator, REE [2], in the "*Procedimiento de Operación 12.2*" dated on October 2018 [18] [3]

To analyze the plant's performance, the software DigSILENT PowerFactory 2019 will be used to carry out the simulations.

To achieve the aforementioned objective, several stages have to been done previously:

1. Understanding of the interconnection and operating requirements in the Spanish and European grid codes. These include: reactive power compliance, energy quality (harmonics, flicker), active power control, voltage-ride-through (VRT), voltage and frequency ranges.

2. Modelling of a floating photovoltaic plant in the software DigSILENT Power-Factory for electrical studies.

3. Dynamic modelling of solar inverters in PowerFactory. This includes the modelling of the power plant controller (PPC), inverter protections and control systems for dynamic simulations.

4. Interpreting the obtained simulation results to determine the degree of compliance of the connection requirements defined in P.O. 12.2.

---

[2]REE: Red Eléctrica de España. Spanish transmission grid operator

[3]Although it is not yet approved by the MITECO, it unifies the interconnection conditions required to the electricity generation modules for network connection from the Commission Regulation (EU) 2016/631 in force since of 14 April 2016, adapting it to the particular conditions of Spain.

1.5 Structure of the thesis

The present thesis is organized into 6 chapters, with the following contents:

- **Chapter 1**: This is an introductory chapter to the master thesis topic, describing the basics of a floating photovoltaic plant. Additionally, the master thesis objectives are established.

- **Chapter 2**: In this chapter, the network code requirements for the FPV plant grid connection are described, following both the P.O. 12.2 and the Commission Regulation (EU) 2016/631 [19].

- **Chapter 3**: Along this chapter, the steady state studies are carried out. These studies include: power flow, reactive power compliance, short-circuit study and energy quality assessment.

- **Chapter 4**: During this chapter, the dynamic model in PowerFactory of the PV inverters considered will be described.

- **Chapter 5**: Throughout this chapter, dynamic simulations will be carried out, analyzing its performance in accordance with the operation requirements defined in chapter 2.

- **Chapter 6**: Finally, the conclusions obtained along this master thesis are comprised in this chapter. Additionally, alternatives and proposals for improvement in future works will be discussed.

Chapter 2

Grid Interconnection Requirements

The European Commission published on 14th April 2016, the *Commission Regulation (EU) 2016/631* [1], which ensures a security energy supply, facilitating the energy trading between countries, by setting a network code on requirements for the grid connection of power generators [19].

The code establishes different operating conditions for the grid connection of power-generation facilities. Despite of this, each national transmission grid operator must prepare their corresponding network code, complying with the minimum operating requirements defined in Commission Regulation (EU) 2016/631.

In the case of Spain, REE proposed the new P.O. 12.2 [18], setting more restrictive grid connection conditions. Although it is pending of approval, it is expected to enter into force as soon as possible [20]. Therefore, during this thesis, the network connection requirements used, are those considered in the *"Procedimiento de Operación 12.2"* [2], dated on October 2018 and which is available in [18].

---

[1] All EU member countries have a period of 2 years since its publication to adapt their grid codes to the requirements set in the Commission Regulation (EU) 2016/631

[2] After consulting several companies, it is concluded that the P.O. 12.2 is being applied for the plants whose inverters procurement has been made after March 2018.

2.1 Category of the Floating PV plant

First of all, it is necessary to identify the significance of the plant under study. This will determine the different operating conditions that the plant must fulfill. According to the Commission Regulation (EU) 2016/631, the plant's evaluation will depend on the capacity and the voltage level at its point of interconnection (POI/PCC) [19]. The threshold limits may vary depending on the synchronous area where the plant is going to be located and should be arranged. These boundaries should be confirmed by the corresponding Transmission System Operator (TSO).

From Table 1 in [19], Spain belongs to "Continental Europe Area". Hence, four categories can be distinguished in Table 2.1 in accordance with P.O. 12.2.

Table 2.1: Evaluation of the FPV plant category

Category	Power at PCC	Voltage at PCC
A	$0.8 \text{ kW} \leq \text{P} \leq 100 \text{ kW}$	$< 110 \text{ kV}$
B	$100 \text{ kW} \leq \text{P} \leq 5 \text{ MW}$	$< 110 \text{ kV}$
C	$5 \text{ MW} \leq \text{P} \leq 50 \text{ MW}$	$< 110 \text{ kV}$
D	$\text{P} < 50 \text{ MW}$	$\geq 110 \text{ kV}$

The point of interconnection for the FPV plant, will be a 132/220 kV substation from Iberdrola S.A. Therefore, from Table 2.1, the category of the plant is deduced to be type D. Thus, following connection and operating requirements must be referred to power-generating modules of type D, in accordance with the prerequisites defined in [18] and [19].

2.2 Energy Quality

The evaluation of energy quality consists on the measurement of the main electrical waveforms (voltage and current) at the PCC. To analyze the quality of the power injected to the electrical system, it will be considered the following studies: flicker, harmonic distortion and voltage phase unbalance.

During section 2.2.1, the planning levels for the energy quality are referred to section 4.1.2 from P.O. 12.2 [18]. These levels are treated as reference values to ensure the electromagnetic compatibility of the plant.

2.2.1 Voltage disturbance planning levels

- **Flicker**: the flicker planning levels are the ones set in the IEC 61000-3-7 [21], with the following values:

    - $P_{st} \leq 1.0$

    - $P_{lt} \leq 0.8$

- **Harmonics**: with the aim of ensuring a good waveform quality, the planning levels corresponding to the voltage harmonic content are set in IEC 61000-3-6 [22] and are pointed out in Table 2.2. Therefore, the voltage harmonic content

Table 2.2: Voltage harmonic planning levels at grid interconnection points

Odd Harmonics				Even Harmonics	
no multiple of 3		multiple of 3			
Harmonic order	Harmonic voltage (%)	Harmonic order	Harmonic voltage (%)	Harmonic order	Harmonic voltage (%)
5	2	3	2	2	1.4
7	2	9	1	4	0.8
11	1.5	15	0.3	6	0.4
13	1.5	21	0.2	8	0.4
$17 \leq n \leq 49$	$1.2 \cdot \frac{17}{n}$	$21 < n \leq 45$	0.2	$10 \leq n \leq 50$	$0.19 \cdot \frac{10}{n} + 0.16$
Total Harmonic Distortion (THD) : 3.00 %					

at each frequency should be lower than the defined limits. In addition, voltage Total Harmonic Distortion (THD) must be lower than 3.00 %. Otherwise, an harmonic filter is needed.

- **Voltage phase unbalance**: according to IEC 61000-3-13 [23], the degree of

unbalance (μ) is measured in %, is the ratio of the negative sequence voltage and the positive sequence voltage. Thus, the planning levels are set to:

- $\mu \leq 1\%$ for short duration level

- $\mu \leq 2\%$ for very short duration level

2.3 Frequency Requirements

In this section, the technical requirements regarding to frequency variations that the FPV plant must satisfy are described. General requirements are established in *Article 22* from the Commission Regulation (EU) 2016/631 [19], to guarantee the safety and control of the whole electrical system.

2.3.1 Frequency ranges

Frequency variations can cause important consequences to the performance of the power plant. For this reason, the TSO must define operating frequency ranges in which the plant must remain connected to the grid. These frequency boundaries are defined in Table 2.3.

Table 2.3: Minimum operating time periods as function of the grid frequency

Frequency Range [Hz]	Operation time period
47.5 - 48.5	30 minutes
48.5 - 49	unlimited
49 - 51	unlimited
51 - 51.5	30 minutes

However, the values shown in Table 2.3 will depend also on the voltage level at PCC. Therefore, figure 2-1 represents the minimum time periods that the plant must remain connected at different frequencies and voltage levels at the PCC. When the operating conditions (V_{PCC} and frequency) are inside the *red* boundary, the plant could operate unlimited. However, if the operating point moves out this boundary,
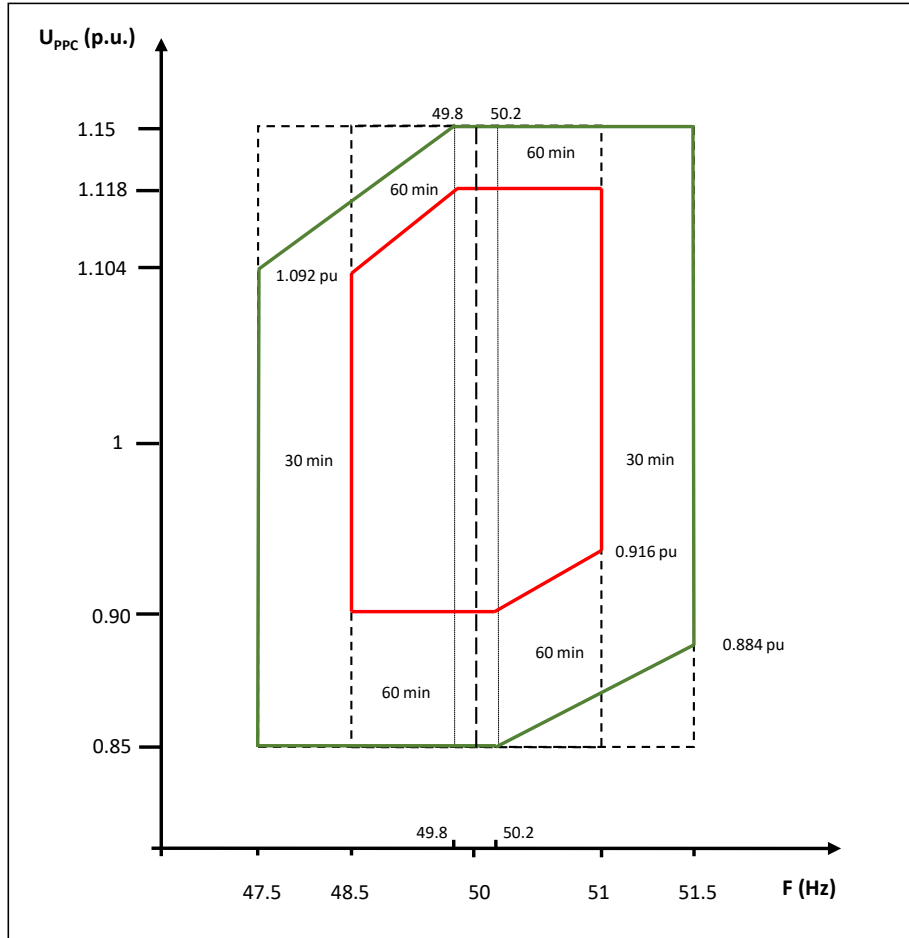
Figure 2-1: Operating time periods of the plant at different frequency values when the voltage level at PCC is between 110 kV and 300 kV

but still is inside the *green* one, the plant must remain connected 30 or 60 minutes, according to the operating conditions. Outside the green threshold, the plant must be disconnected from the grid.

2.3.2 Regulation mode power-frequency limited - overfrequency (MRPFL-O)

The power generating modules must be capable of activating their active power-frequency control following the criteria defined by the TSO. As defined in P.O. 12.2, control activation frequency is set to 50.2 Hz with an statism of 5%.

2.3.3 Regulation mode power-frequency limited - underfrequency (MRPFL-U)

Similarly for the overfrequency condition, the power generating modules must manage the active power when the frequency decreases. In the P.O. 12.2, the control activation frequency is set to 49.8 Hz with an statism of 5%.

2.4 Voltage requirements

2.4.1 Voltage ranges

As the FPV plant has category D, the power plant controller (PPC) should be able to regulate the power generating modules to withstand the voltage levels compressed in Table 2.4, extracted from PO.12.2. These values are in accordance with the voltage limits of table 1 from the Commission Regulation (EU) 2016/631 [19].

Table 2.4: Minimum operation time periods when voltage level at PCC is between 110 kV and 300 kV

Voltage Range [pu]	Operation Time
0.85 - 0.90	60 min
0.90 - 1.118	unlimited
1.118 - 1.15	60 min

Thus, the maximum voltage at PCC that can be withstand is 1.15 pu during one hour. This maximum voltage will set the boundary to identify possible over-voltages in the system. On the other hand, the minimum voltage so that the plant remains under operation is set to 0.85 pu for one hour. If the voltage goes below V_{min}, a low voltage-ride-through scenario is identified.

2.4.2 Current injection control

During Voltage-Ride-Through (VRT) conditions, the FPV plant must control the voltage at PCC by injecting or absorbing current. According to section 5.2.3 in the

P.O. 12.2 [18], the current control will be activated if there is a voltage disturbance such that the voltage magnitude at PCC is out of the limits ($V_{min} \leqslant V_{PCC} \leqslant V_{max}$) specified in Table 2.4.

In addition, the following considerations have to be taken into account:

- V_{max} is the maximum voltage considered in Table 2.4 that the plant will support without disconnecting from the grid (1.15 pu)

- V_{min} is the minimum voltage considered in Table 2.4 that the plant will support without disconnecting from the grid (0.85 pu)

2.4.3   Reactive power requirements

The Commission Regulation (EU) 2016/631 defines a boundary for which the power modules shall be capable of injecting/absorbing the required reactive power at its maximum capacity. However, is the TSO who shall specify the reactive power reserves to keep the voltage level at PCC within the requisites.

These boundaries are represented in figure 2-2, which shows the voltage edges at the point of common coupling, complying with the reactive power as function of the maximum power capacity (P_{max}) of the plant. Each TSO shall specify their corresponding U-Q/P_{max} profile, that should be inside the inner envelope included in figure 2-2 [19]. In Spain, the corresponding voltage boundary for the FPV plant under study, is given by the red boundary in figure 2-2. As consequence, the voltage range at the PCC in order to comply with the reactive power requirements is between 0.95 pu and 1.05 pu.

Generally, any power plant operates below its maximum capacity, P_{max} as they are limited to the contracted power. Thus, the plant must comply with the reactive power requirements while ensuring that the voltage level at the point of interconnection stays within the defined threshold. Therefore, boundaries of P-Q/P_{max} profiles, as function of the active power, should also be considered. The black curves from
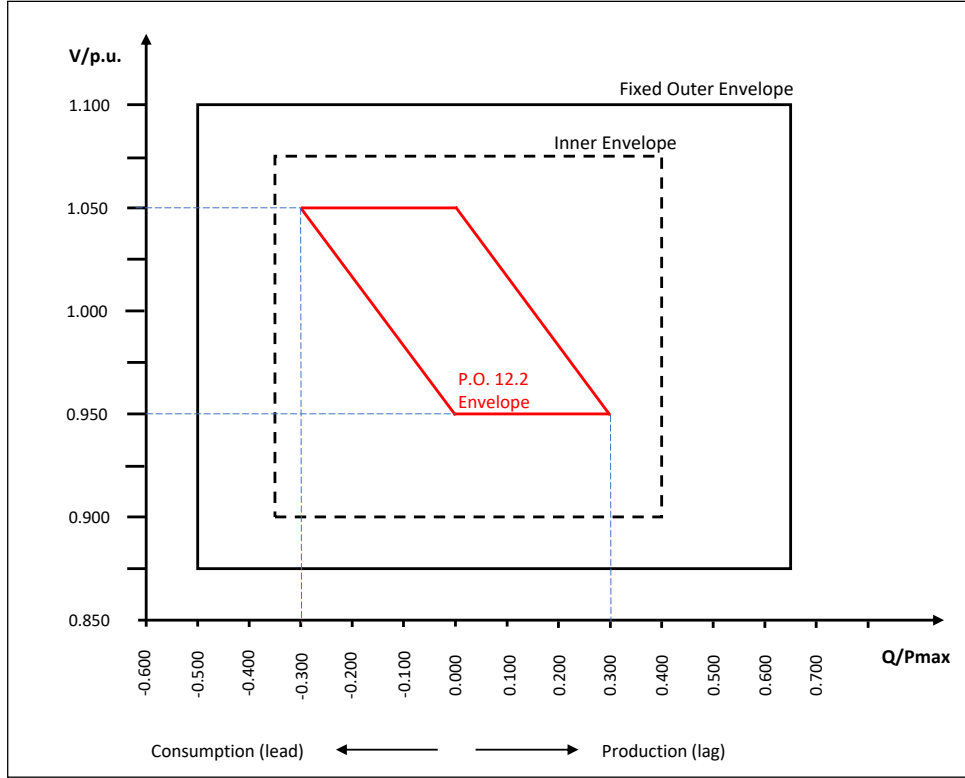
Figure 2-2: U-/Q/Pmax profile for a photovoltaic plant

figure 2-3 are the boundaries set by the Commission Regulation (EU) 2016/631 and the red curve, is the enveloped that applies in P.O. 12.2 [18].

Therefore, the FPV plant should be capable to inject or absorb enough reactive power to comply with the P/Q curve shown in red in figure 2-3, while ensuring that the voltage at PCC is within the limits of figure 2-2. Additionally, from figure 2-3, when the plant is exporting its nominal active power, the plant should manage any operating point within power factor range of 0.958 leading (inductive) to 0.958 lagging (capacitive).

$$\frac{Q}{P_{max}} = 0.300 \tag{2.1}$$

$$cos\phi = cos(atan(0.300)) \approx 0.958 \tag{2.2}$$
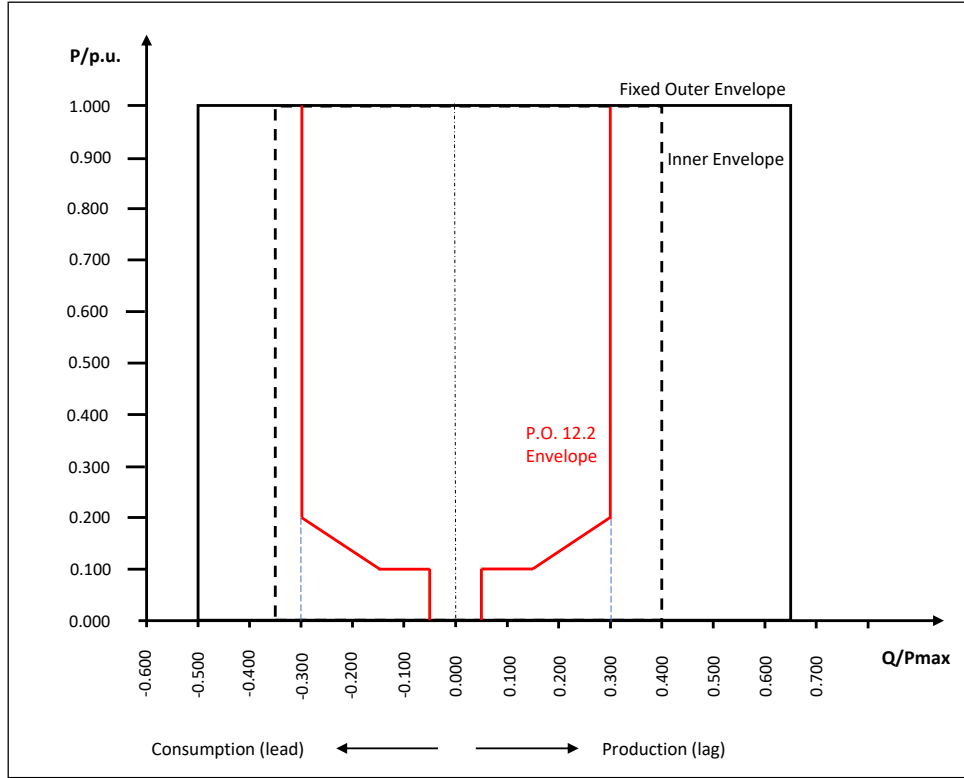
Figure 2-3: P-Q/P_{max} profile for a power park module

2.5 Robustness requirements

2.5.1 Low-voltage ride through (LVRT)

Regarding robustness requirements, during low-voltage situations, the voltage profile at PCC should comply with figure 2-4b. This voltage profile set by REE, can be compared with 2-4a defined in Commission Regulation (EU) 2016/631 [19].

It can be observed that the LVRT profile for the considered FPV plant is more restricted when applying the P.O. 12.2. As result, a LVRT scenario is detected if the voltage at PCC goes down 0.85 pu. In the case that the voltage gets to zero level, the LVRT control mode of the plant will try to recovery it. If the voltage level remains during 150 ms at 0 pu then, the FPV plant must disconnect from the grid.
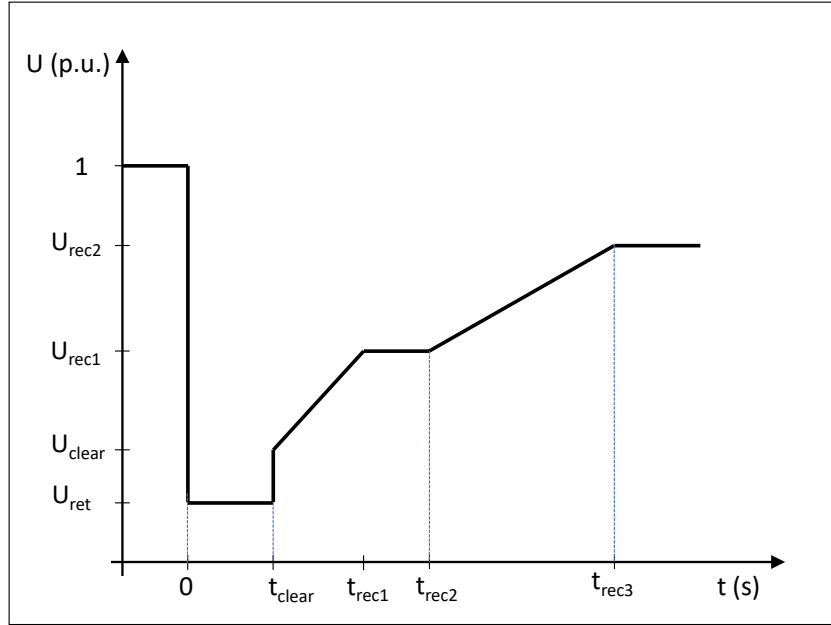
(a) Low voltage ride through profile defined in Commission Regulation (EU) 2016/631
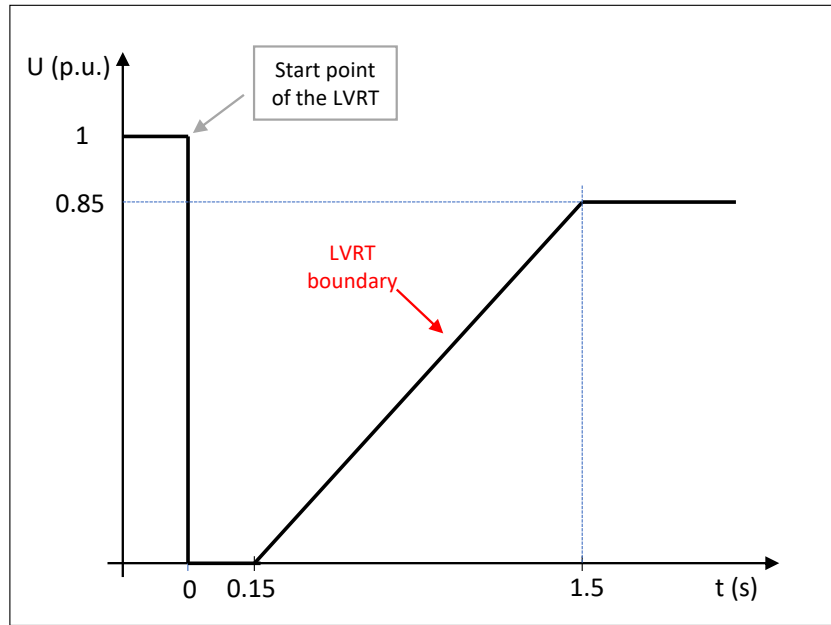
(b) Low voltage ride through profile defined in P.O. 12.2

Figure 2-4: Fault ride through profile for type D photovoltaic plants

Alternatively, the maximum allowed duration for operating with a LVRT condition is 1.5 seconds. After that, the plant must disconnect immediately from the grid. For different low-voltage magnitudes, the control of the protections of the plant must trip according to the curve from figure 2-4b.

2.5.2 Over-voltage ride through (OVRT)

Alternatively, the grid voltage could increase over its operating limits. This will cause an over-voltage ride through (OVRT) scenario. In consonance with section 5.3.3 in [18], the floating photovoltaic plant should be capable of remaining connected and operating in steady state inside the OVRT boundary included figure 2-5.
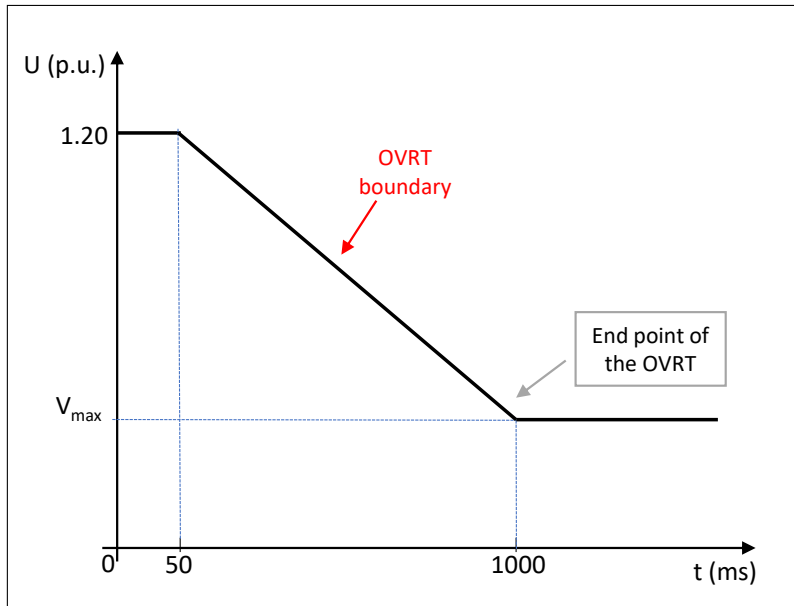
Figure 2-5: Over-Voltage Ride Through profile

The protections in the plant will detect an overvoltage if the voltage at PCC exceeds V_{max}, which has been defined in Table 2.4 to be 1.15 pu. If the overvoltage increases over 1.20 pu then, the plant must disconnect immediately. For voltage levels between V_{max} and 1.20 pu, the voltage profile from figure 2-5 must be followed to avoid grid disconnection.

Chapter 3

Steady State Results

3.1   Modelling of the FPV plant

The present study considers an existing electrical network as well as its corresponding system to which the floating PV plant is connected. The voltage at PCC is 132 kV, corresponding to the voltage level of the Iberdrola's switching substation. An equivalent single line diagram of the plant is presented in figure 3-1. For a more detailed representation, the reader can consult the diagram included in Appendix C.

The nominal capacity of the FPV plant is 50 MW, consisting of a total of 16 central inverters up to 58 MVA@40°C of nominal power coupled to the PCC. The inverters are the model *HEMK 660V FS3510K* from Power Electronics (PE). It should be mentioned that the size of the inverters has no impact on the conclusions, since it is a common practice to apply equivalence power flow and dynamic models to reduce data assimilation. However, for a complete explanation of how to model a photovoltaic plant, the document *WECC Guide for Representation of Photovoltaic Systems in Large-Scale Load Flow Simulations* [24] can be consulted.

For each inverter, an associated two winding step-up transformer (rated to 3.8 MVA) rises the voltage from the LV terminal up to 30 kV as seen in figure 3-1. The generation units, are divided in 4 medium voltage (MV) collector circuits, with four
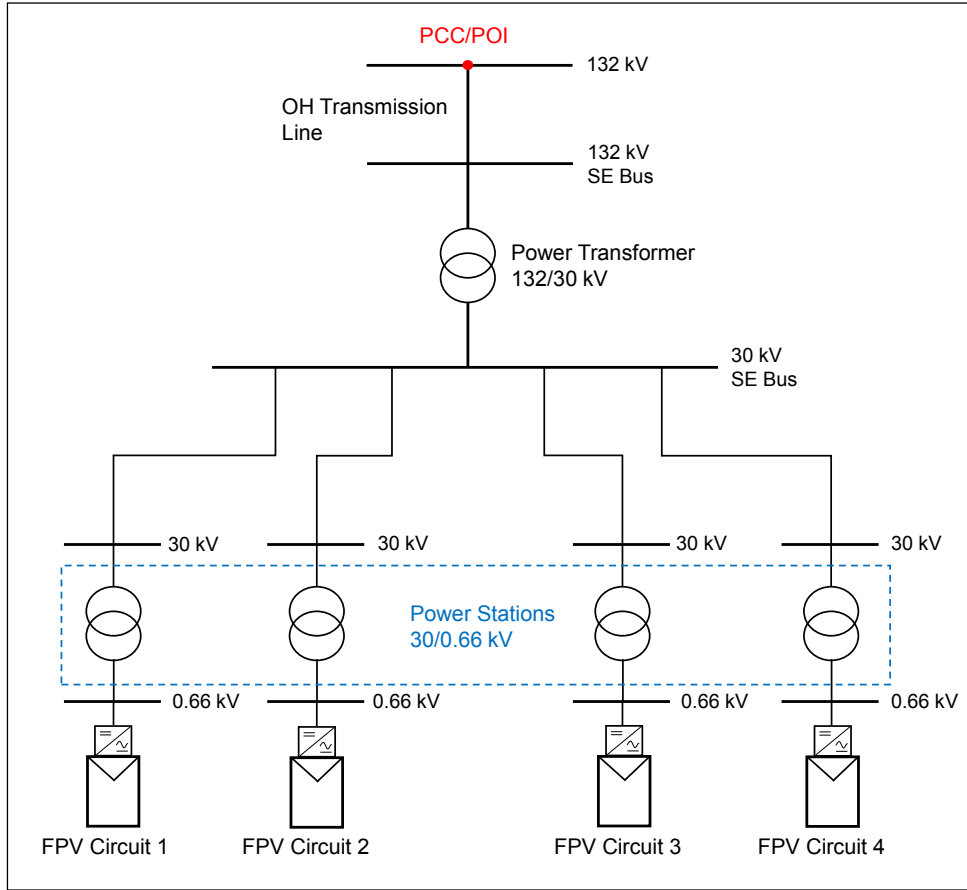
Figure 3-1: Floating Photovoltaic plant equivalent single line diagram

power stations per circuit. A 15 km overhead (OV) high voltage transmission line will connect the step-up plant's substation with the point of interconnection.

The FPV plant incorporates a Power Plant Controller (PPC) responsible in turn for managing the reactive power contribution of the FPV plant at the PCC [24], [25]. The PPC will control the generation units to fulfill with the operating requirements.

All the technical data of the electrical equipment needed to model the plant is included in Appendix A.

3.2 Load Flow Studies

The load flow studies are undertaken to examine most demanding scenarios set in P.O. 12.2. These scenarios can be identified in section 2-3 and 2-4 of the present document. Also, the power flow study serves for analyzing the maximum circuit and transformer loading conditions and voltage profile across the studied network.

The operating voltage ranges at the PCC in which the FPV should control the reactive power, were defined in figure 2-2, to vary between 0.95 pu and 1.05 pu. So then, if the nominal voltage level is 132 kV, the steady state voltages considered during the studies are between 125.4 kV and 138.6 kV.

The power ratings of all the inverter stations should be enough to guarantee the contracted active power at the PCC while complying with the reactive power flow. Moreover, the electrical equipment should be capable of exporting/importing the maximum power from/to all inverter station units, without exceeding the thermal ratings of the cable circuits and inverter transformers.
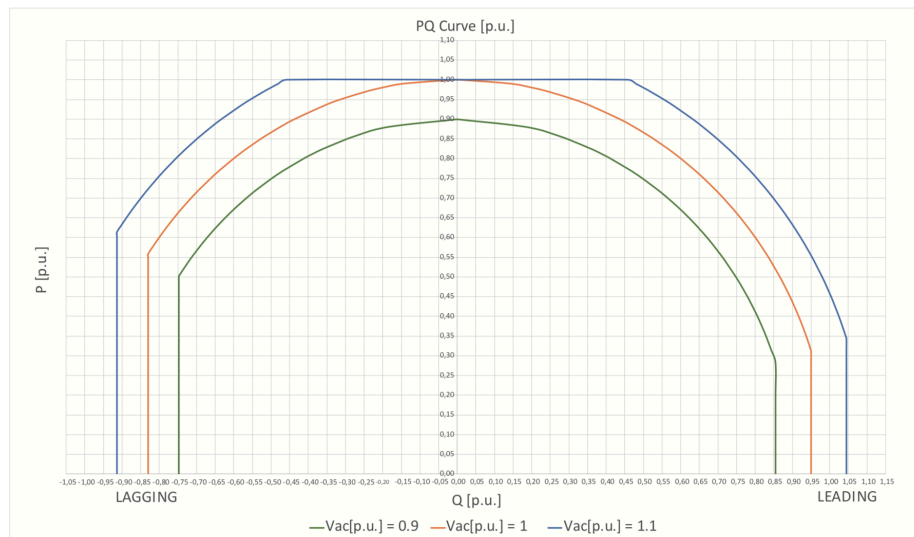
Figure 3-2: HEMK inverter reactive power capability curve

41

In order to meet the reactive power requirements, the plant has been designed including only one source of reactive power, that are the PV inverters. According to the data sheet provided by Power Electronics [26], the inverter can operate continuously anywhere within the area below the curves from figure 3-2. The figure corresponds to the reactive power capability curve for different voltage levels at its terminal.

Since the power factor may vary from 0.958 inductive to 0.958 capacitive, the following two operating conditions are expected to result in onerous loading conditions for the plant:

1. exporting Q_{max} with power factor 0.958 inductive and voltage 1.05 pu at PCC;

2. importing Q_{max} with power factor 0.958 capacitive and voltage 0.95 pu at PCC.

3.2.1 Power Flow Sign convention

In order analyze the power flow results, it is recommended to establish a sign convention for the power flow and to be consistent throughout the studies. For this thesis, *Generator Convention* is applied, where active power output from a generator has positive flow. In PowerFactory, both FPV inverters and the external grid are managed as generators [27]. Therefore, the direction of the power flow will be as the one presented in figure 3-3.
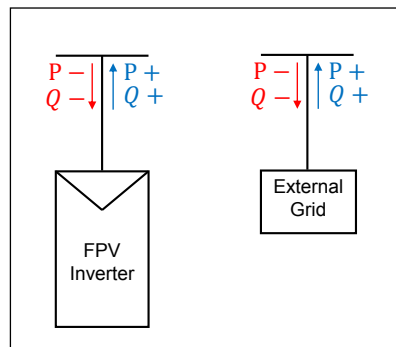
Figure 3-3: Active/Reactive power flow sign convention

When the power factor at the external grid is *lagging* then, reactive power flow is out of the generator, i.e. out of the inverters, and is considered to be positive flow

in the same direction as active power flow. Consequently, the inverter is producing reactive power (capacitive).

Alternatively, a *leading* power factor means that reactive power flow is going into the generator and considered to be negative flow, i.e., with opposite direction than active power flow. As the generator is absorbing reactive power, it is treated as an inductive element.

Additionally, if the operating condition is with unity power factor then, there is no reactive power flow from or out of the generation sources.

3.2.2 Initial Conditions

Before starting with the power flow study, specific operating conditions for the plant must be defined.

- The on-load tap changer of the power transformer from the FPV plant's 132/30 kV substation is activated to automatically control the voltage at the MV terminal. The tap changer is located in the primary winding at the high voltage side of the transformer and it is set to fix a voltage level of 1 pu at the 30 kV SE Terminal (see Appendix C).

- At the power station transformers (30/0.66 kV), the tap position is fixed at its neutral position (tap = 0).

- The reactive power injected/absorbed by the inverters is limited such that the voltage at their terminals do not exceed the operating voltage limits (0.90 pu - 1.10 pu). These limits are given by the inverters reactive power capability shown in figure 3-2.

3.2.3 Power Flow Results

This section presents the results of the power flows considered in this study. The selected operating scenarios correspond to the most restrictive operating conditions identified in the network code. Besides the local normative, also the standards IEEE Std 141 [28] and IEEE Std 399 [29] are specifically applied for the calculation of the power flows. Additionally, two more scenarios have been added, corresponding to a voltage level at PCC of 1 pu.

The nomenclature to identify each power flow scenario is the following:

- Scenario A: $U_{PCC} = 0.95$ pu. - $\cos \phi = 0.958$ capacitive

- Scenario B: $U_{PCC} = 0.95$ pu. - $\cos \phi = 0.958$ inductive

- Scenario C: $U_{PCC} = 1$ pu. - $\cos \phi = 0.958$ capacitive

- Scenario D: $U_{PCC} = 1$ pu. - $\cos \phi = 0.958$ inductive

- Scenario E: $U_{PCC} = 1.05$ pu. - $\cos \phi = 0.958$ capacitive

- Scenario F: $U_{PCC} = 1.05$ pu. - $\cos \phi = 0.958$ capacitive

Power flow results are comprised in Table 3.1, which represents the voltage profiles, and Table 3.2 which shows the thermal loading of the conductors and power transformer.

From Table 3.1, it can be observed that the FPV plant voltage ranges from 1 pu to 1.0404 pu at the inverter terminals and the voltage at the 30 kV terminals from the power stations is stabilized around 1 pu. Therefore, all voltages are within the continuous operating limits, that were considered to be $\pm$ 10% of nominal voltage for all scenarios considered.

Table 3.1: Voltage profile of FPV plant under different operating conditions

Scenario	V_{PCC} [pu]	Inverters [pu] Max	Min	PS Terminals [pu] Max	Min	30kV ST Terminal	Transformer Tap Position
A	0.95	1.0054	1.0041	1.0057	1.0044	1.0064	-6
B	0.95	1.0391	1.0370	1.0046	1.0024	1.0007	0
C	1	1.0037	1.0023	1.0042	1.0028	1.0010	-2
D	1	1.0398	1.0377	1.0055	1.0034	1.0017	4
E	1.05	1.0021	1.0007	1.0028	1.0014	1.0005	2
F	1.05	1.0404	1.0383	1.0064	1.0043	1.0026	8

On the other hand, Table 3.2 gives the thermal loading's of the lines and substation transformer. It is observed that the loading of the collector circuits can be up to 55.5% loading, which still has enough margin until reaching the current capacity of the cables. The loading in the transmission line varies depending on the operating

Table 3.2: Electrical equipment loading's of FPV plant under different operating conditions

Scenario	V_{PCC} [pu]	Power Factor	MV lines [%] Max	Min	HV Line [%]	Substation Transformer [%]
A	0.95	capacitive	51.909	21.092	30.157	91.90
B	0.95	inductive	55.760	22.613	30.048	91.50
C	1	capacitive	52.084	21.170	28.711	87.50
D	1	inductive	55.593	22.545	28.542	91.20
E	1.05	capacitive	52.076	21.617	27.306	85.30
F	1.05	inductive	55.434	22.481	27.178	91.00

conditions, achieving a maximum thermal loading of 30.16 % in scenario A. Moreover, the power transformer, rated at 60 MVA, has enough capacity to withstand the most demanding scenarios without overloading[1].

_____

[1]Generally, power transformer have temporary overloading capability.

3.3 Reactive Power Capability Study

Another important study is to determine if the plant has reactive power capability to comply with the required conditions defined in P.O. 12.2 [18]. Thus, several PQ assessments at the point of common coupling have been carried out for different voltage levels.

It was assumed that the power factor at the PCC varies from 0.958 inductive to 0.958 capacitive and the tap position of the 132/30 kV transformer is automatically adjusted to maintain a voltage level of 1.00 pu at the 30 kV terminal of the substation. Common voltage levels for MV terminals are between 0.90 pu and 1.10 pu.

The FPV plant has been modelled as in figure C-1, where each component of the system has been defined according to their operating characteristics. The inverters are supposed to operate within their capability curve shown in figure 3-2, in order to maximize the output power under the most unfavourable operating conditions.

3.3.1 PQ Curve at $U_{PCC} = 0.95$ pu

In figure 3-4, the PQ curve of the floating PV plant is showed when the voltage level at the point of interconnection is 0.95 pu. The blue line represents the PQ power requirements established in P.O. 12.2 and the red line represents the threshold limits that the plant may potentially achieve if the solar resource is enough.

It can be noticed that the FPV plant is able to achieve any requested operating scenario at $V_{PCC} = 0.95pu$ with a power factor varying from 0.958 inductive to 0.958 capacitive.

46
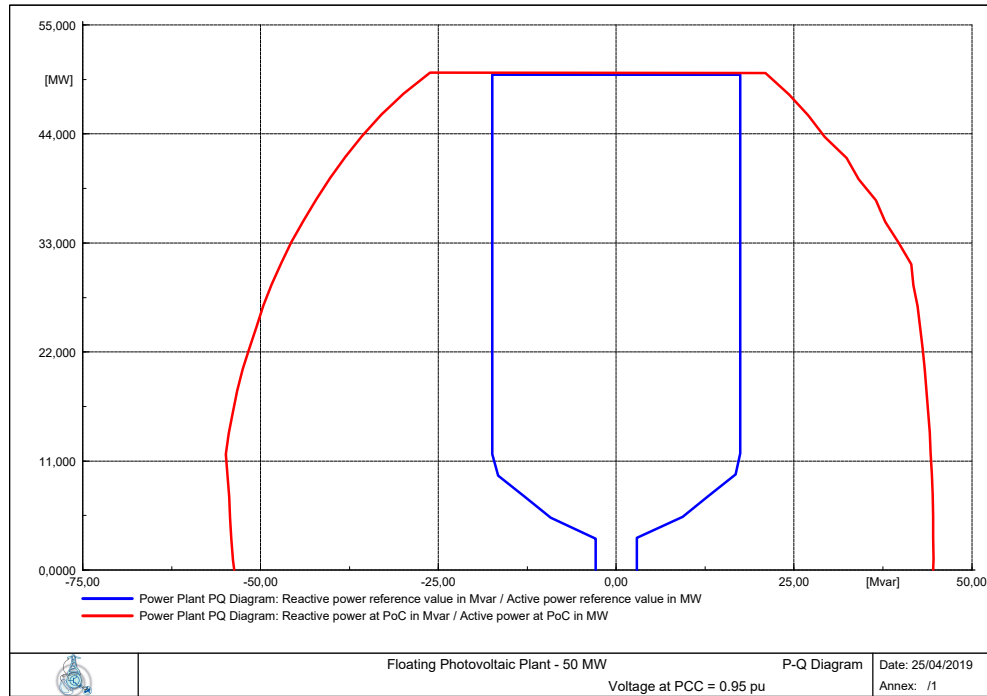
Figure 3-4: PQ curve at 0.95 pu voltage at PCC

3.3.2 PQ Curve at $U_{PCC} = 1.00$ pu

Similarly, figure 3-5 represents the reactive power capability when the voltage level at PCC is 1.00 pu. The inverters have enough reactive power capacity to meet the reactive requirements.

3.3.3 PQ Curve at $U_{PCC} = 1.05$ pu

The remaining scenario required by P.O. 12.2 to analyze the reactive power compliance is when the voltage level at PCC is 1.05 pu. In the same way as previous scenarios, several load flows were made varying the power factor from 0.958 inductive to 0.958 capacitive, to analyze the reactive power of the plant. Figure 3-6 shows that the plant is able to inject/absorb the required reactive power according to the requirements established by the transmission grid operator.

Therefore, it can be observed that the most onerous condition for the FPV plant to meet the reactive power requirement (blue curve) corresponds to figure 3-4, when
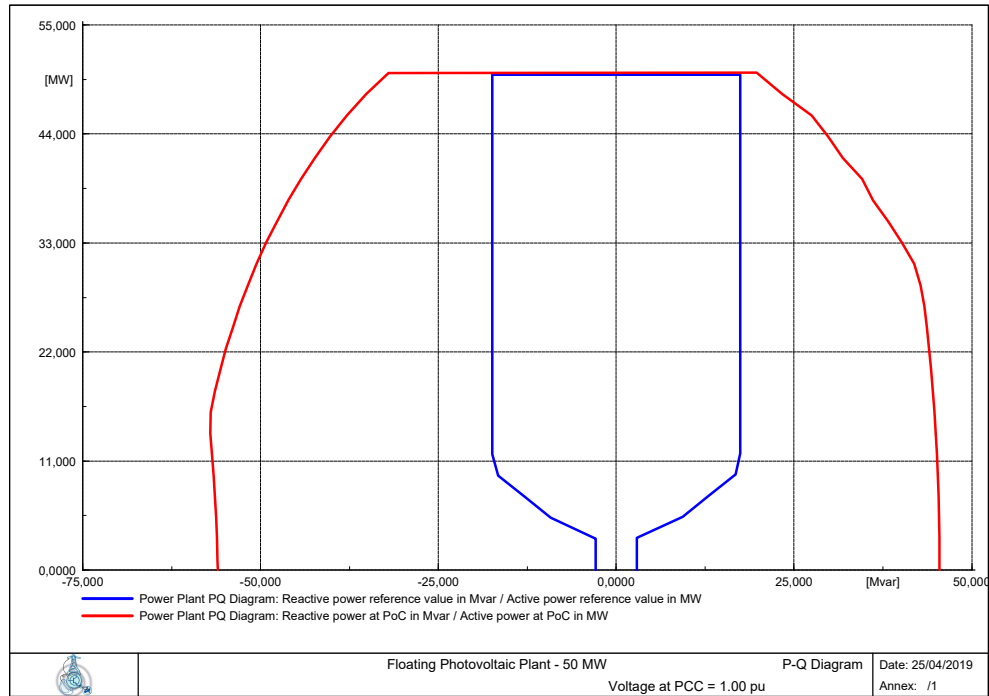
Figure 3-5: PQ curve at 1 pu voltage at PCC

the voltage at the PCC is at 0.95 pu while maintaining 0.958 lagging power factor at the PCC.

Consequently, since the reactive power capability curves enclose the reactive power requirements, the proposed design does not need additional reactive compensation elements.

3.4 Short-Circuit Analysis

The short-circuit study is developed based on the regulation IEC 60909-0 [30], considering the following types of short-circuits:

1. Three phase short-circuit

2. Two-phase short-circuit

3. Two-phase to ground short-circuit

4. Single phase to ground short-circuit

48
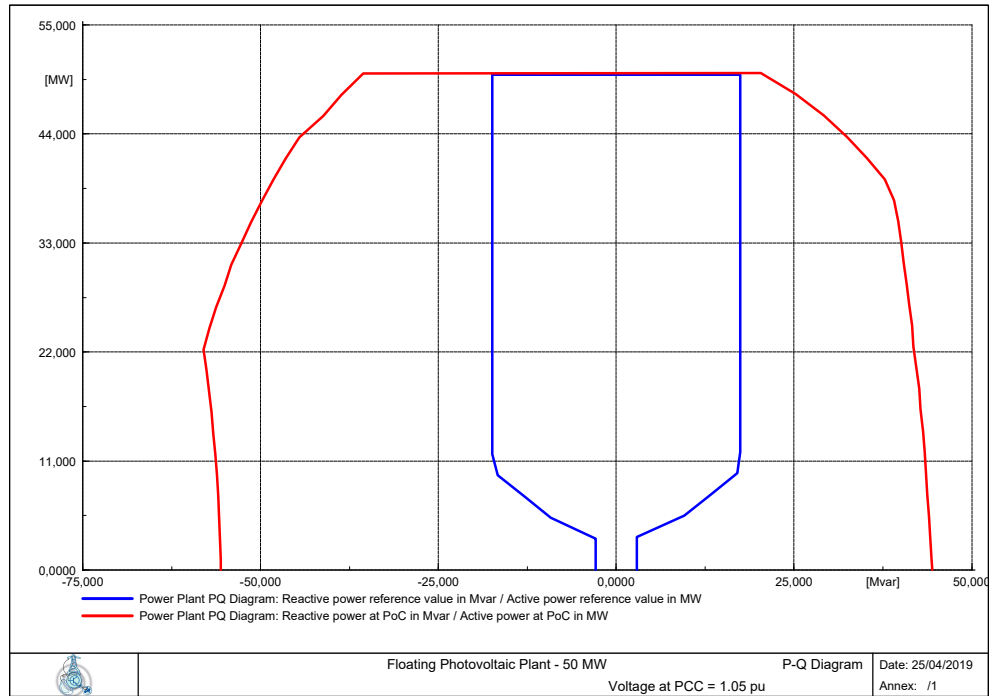
Figure 3-6: PQ curve at 1.05 pu voltage at PCC

The IEC 60909 is based on the nominal dimensions of the operating point of a system and uses correction factors for voltages and impedance to deploy conservative results. For the calculation of the maximum short-circuit currents, an overvoltage factor of 1.1 at the MV terminals is assumed.

The short-circuit currents in the FPV plant are calculated to:

- Measure the ability of circuit breakers or any protection devices to interrupt fault currents

- Check the ability of all equipment on the system to withstand the mechanical forces associated with such fault currents

The short-circuit base case uses all available generation to ensure that the maximum possible current level is achieved. For this project, the short-circuit fault level of the grid has been assumed as a mean value for 132 kV voltage levels, to be 15 kA[2].

---

[2]This value has been obtained from a Spanish utility. Generally, the owner of the POI bus should provide information about its short-circuit contributions.

Out of the short-circuit study, it is possible to conclude that the ratings of the involved equipment shall withstand at a minimum, the following short-circuits currents, expressed in Table 3.3.

Table 3.3: Maximum short-circuits currents

Three Phase short-circuit			
	Ik" (kA)	Ib (kA)	Ip (kA)
132 kV	15.248	15.248	37.652
30 kV	9.150	9.150	23.415
0.660 kV	49.375	49.375	117.499
Two Phase short-circuit			
	Ik" (kA)	Ib (kA)	Ip (kA)
132 kV	12.990	12.990	32.076
30 kV	6.848	6.848	17.638
0.660 kV	38.714	38.831	92.275
Two Phase to ground short-circuit			
	Ik" (kA)	Ib (kA)	Ip (kA)
132 kV	15.281	15.281	37.038
30 kV	6.870	6.870	17.655
0.660 kV	38.831	38.831	92.275
Single Phase to ground short-circuit			
	Ik" (kA)	Ib (kA)	Ip (kA)
132 kV	15.468	15.468	37.038
30 kV	1.067	1.067	2.619
0.660 kV	0	0	0

3.5 Energy Quality Study

3.5.1 Flicker Assessment

A guidance to set the limits for flicker emissions resulting from the connection of new loads is provided by *Engineering Recommendation (ER) P28* in [31]. In general, the severity of flicker values in a FPV plant for short term flicker (P_{st}) and long term flicker (P_{lt}) are inversely proportional to the network fault level.

According to ER P28, for a planning assessment it is recommended a limit of 1 for P_{st} and 0.8 P_{lt}, that matches with the limits defined in section 2.2. Referring to IEC 61400-21 [32], two types of flicker emissions can be identified:

Flicker during continuous operation

The flicker emissions from a static generator during continuous operation are defined as the normal operation of an inverter, excluding the "cut-in" and "cut-off" operations. The flicker results are shown as continuous flicker short-term severity (P_{st}) value and long-term severity (P_{lt}). The short-term and long-term flicker factors during continuous operation are mathematically described by equation 3.1.

$$P_{st} = P_{lt} = c(\psi_k, v_a) \cdot \frac{S_n}{S_k} \tag{3.1}$$

where c is the flicker coefficient, ψ_k is the grid impedance angle, S_n is the rated apparent power of the inverter and S_k is the short-circuit power of the grid.

Flicker during switching operation

The flicker emissions from PV generators during switching operations can be defined as the operation of the inverter during cut-in and cut-off. The flicker switching results are shown as P_{st} and P_{lt}. The short-term flicker disturbance factor during switching

51

operation is defined as in equation 3.2.

$$P_{st} = 18 \cdot N_{10}^{0.31} \cdot k_f(\psi_k) \cdot \frac{S_n}{S_k} \quad (3.2)$$

where N_{10} is defined as the number of switching operations in 10 minutes and k_f is the flicker step factor.

Alternatively, the long-term flicker disturbance factor is given by equation 3.3.

$$P_{lt} = 8 \cdot N_{120}^{0.31} \cdot k_f(\psi_k) \cdot \frac{S_n}{S_k} \quad (3.3)$$

where N_{120} is defined as the number of switching operations in 120 minutes and k_f is the flicker step factor.

3.5.2 Flicker Results

All calculations were undertaken for flicker emission assessment at the PCC for different voltage levels (0.95 pu, 1.00 pu and 1.05 pu), following the methodology provided in IEC 61400-21 [32].

Based on the flicker coefficients for the inverters given by the manufacturer [34] and the short-circuit current at PCC, flicker emission assessment can be computed. The values obtained for short term flicker (P_{st}) and long term flicker (P_{lt}) are presented in Table 3.4.

Table 3.4: FPV flicker results for different voltage levels at PCC

	$U_{PCC} = 0.95$ pu	$U_{PCC} = 1.00$ pu	$U_{PCC} = 1.05$ pu
Pst_{cont}	0.0045932	0.0043745	0.0041757
Plt_{cont}	0.0045932	0.0043745	0.0041757
Pst_{sw}	0.0123618	0.0117730	0.0112377
Plt_{sw}	0.0118699	0.0113045	0.0107904

The maximum flicker during continuous operation is $Pst_{cont} = 0.0045932$ and for switching operation $Pst_{sw} = 0.0123618$. Since these values are lower than the planning limits in P.O. 12.2 then, no significant voltage fluctuation distortion is expected.

3.6   Harmonic Study

The harmonic voltage and current distortion levels are determined based on representative harmonic current injection levels provided by PE [33]. The objectives of the harmonic study are to:

1. determine possible resonance frequencies of the FPV plant under different operating conditions;

2. determine the impact of the resonance conditions in the FPV plant on the individual and total harmonic voltage distortion levels at the PCC.

Voltage harmonic distortion results at PCC are presented by means of a bar diagram, where solid bars in red represents the percentage harmonic voltage for each individual harmonic at the point of common coupling. The striped bar represents the threshold limits according to IEC 61000-3-6, that were expressed in Table 2.2. This standard proposes a *second summation law*, mathematically described by equation 3.4.

$$U_h = \sqrt[\infty]{\sum_{m=0}^{N} U_{h,m}^{\infty}} \tag{3.4}$$

where U_h is the harmonic voltage obtained from aggregating all N generation sources of harmonic order h.

With the IEC 61000-3-6, negative sequence and zero-sequence harmonics are considered into the positive sequence. Therefore, the highest voltage harmonic distortion is achieved, obtaining the worst scenario for the voltage harmonic distortion.

Additionally, the voltage Total Harmonic Distortion (THD) will be calculated. It is defined mathematically by equation (3.5)

$$THD = \frac{\sqrt{V_2^2 + V_3^2 + V_4^2 + ... + V_n^2}}{V_1} \tag{3.5}$$

where

- THD: Total Harmonic Distortion

- V_n: Voltage magnitude for each harmonic component

- V_1: Fundamental voltage component

3.6.1 Resonance analysis

A frequency scan of the floating FPV plant impedance, as viewed from the 132 kV PCC terminal, has been performed to identify any possible harmonic resonance that could appear under different operating conditions. Peaks (poles) and troughs (zeros) can be generated in the impedance frequency at different harmonic frequencies by the capacitance of the collector system cables, transformer and transmission system inductance. Poles create resonance points that could result in very high voltage distortion if an harmonic excitation current is applied at that same frequency from a source, such as the PV inverters. On the other hand, zeros create resonance points that can attract harmonic currents of that same frequency if it exists.

The impedance-frequency scan was assessed to identify harmonic resonance magnitudes and frequencies at which they might appear. Figure 3-7 shows the resulting network impedance up to the 50th harmonic. It can be observed that the connection of the FPV plant could create a parallel resonance close to 29th harmonic order. However, since there is not high harmonic current injection from the inverters at the same frequency, it is not expected to generate significant voltage waveform disturbances at PCC.
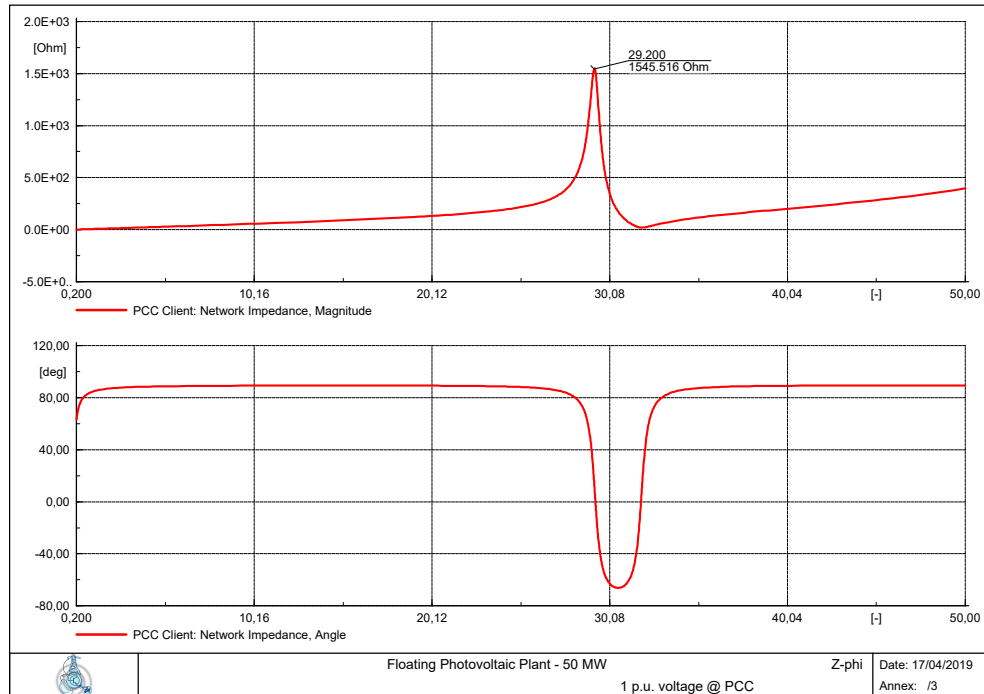
Figure 3-7: Frequency scan of network impedance at PCC at 132 kV

3.6.2 Voltage Distortion Analysis

Voltage harmonic distortion analysis is typically performed to evaluate the severity of any resonance condition identified in the resonance analysis. During the analysis, it has been considered the FPV plant to export 50 MW to the grid, with a 0.958 lagging power factor, corresponding to most unfavourable condition.

Distortion analysis at $U_{PCC} = 0.95$ pu

The voltage distortion result when the voltage level at PCC is 0.95 pu is shown in figure 3-8. As it is observed, for each individual harmonic, the required harmonic levels are satisfied.
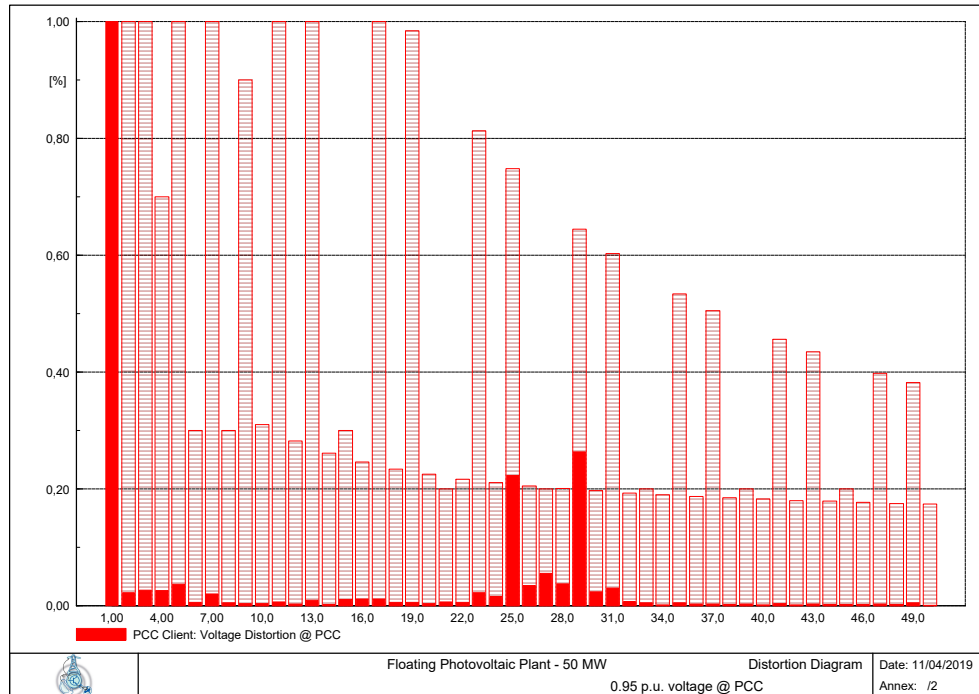
Figure 3-8: Voltage distortion analysis of the FPV plant @PCC 0.95 pu

Distortion analysis at $U_{PCC} = 1$ pu

Similarly, figure 3-5 shows the voltage distortion when the voltage level at the external grid is 1 pu.

No individual harmonics have been detected above the allowed values.

Distortion analysis at $U_{PCC} = 1.05$ pu

At last, figure 3-10 presents the results of the voltage distortion when the PCC voltage is at 1.05 pu. As in previous operating scenarios, from figure 3-10 it is deduced that the individual harmonics are within the limits defined by P.O. 12.2.

Therefore, since the harmonic voltage levels of the FPV complies with the limits then, also fulfills with the harmonic voltage levels set the Commission Regulation (EU) 2016/631. The resonance pole identified in figure 3-7 along with the harmonic voltages, result in a very limited harmonic voltage distortion, meeting in any case with the harmonic thresholds set for the plant.

56
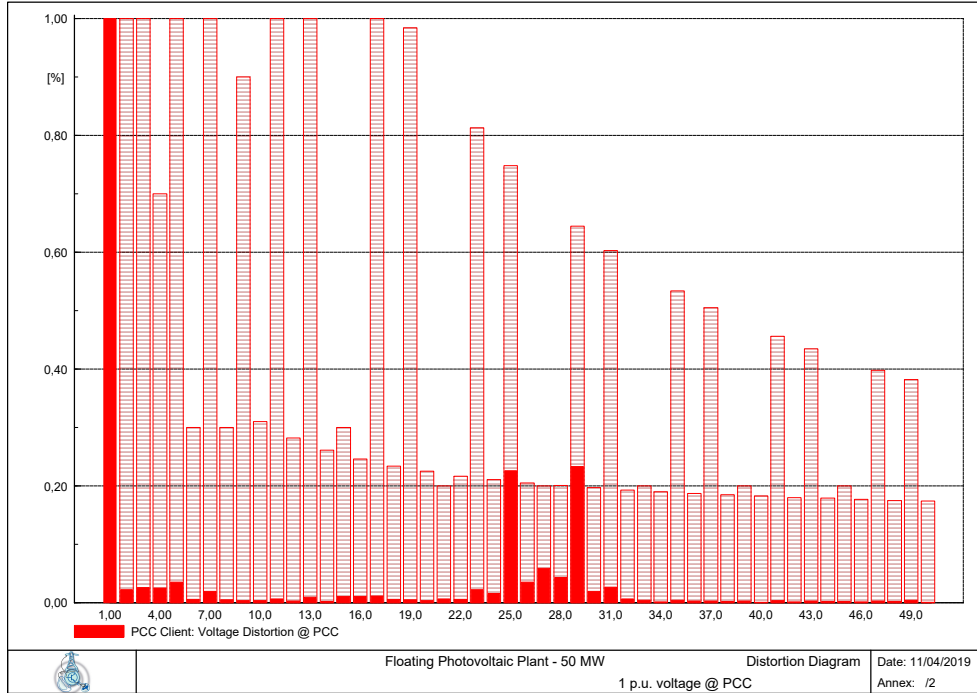
Figure 3-9: Voltage distortion analysis of the FPV plant @PCC 1 pu

Additionally, Table 3.5 collects the resulting Total Harmonic Distortion (THD) for the different voltage levels.

Table 3.5: Voltage THD results for different voltage levels at PCC

Scenario	Voltage THD
$U_{PCC} = 0.95$ pu	0.3632 %
$U_{PCC} = 1.00$ pu	0.2559 %
$U_{PCC} = 1.05$ pu	0.2099 %

Since the maximum voltage THD obtained is **0.3632** %, which is quite below the planning limits specified in Table 2.2 (3.00 %), it can be concluded that the energy quality of the FPV stays within all the required limits.

The resultant FPV harmonic assessment can be translated to the voltage and current waveforms distortion shown in figure 3-11. In the top plot, it can be seen that the voltage distortion is practically negligible corresponding to a low voltage Total Harmonic Distortion value.

57
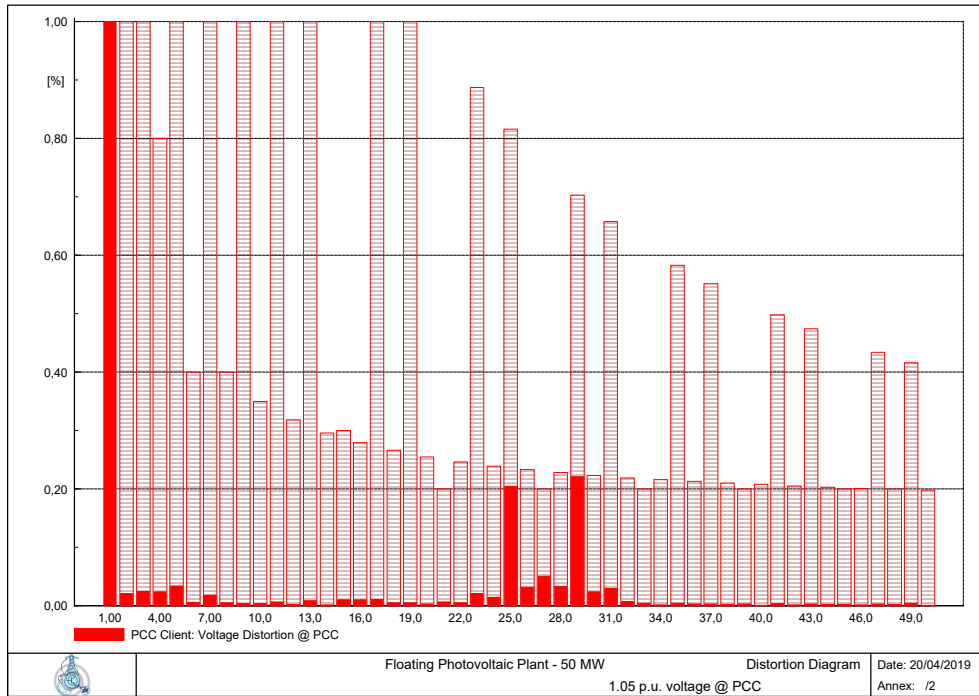
Figure 3-10: Voltage distortion analysis of the FPV plant @PCC 1.05 pu
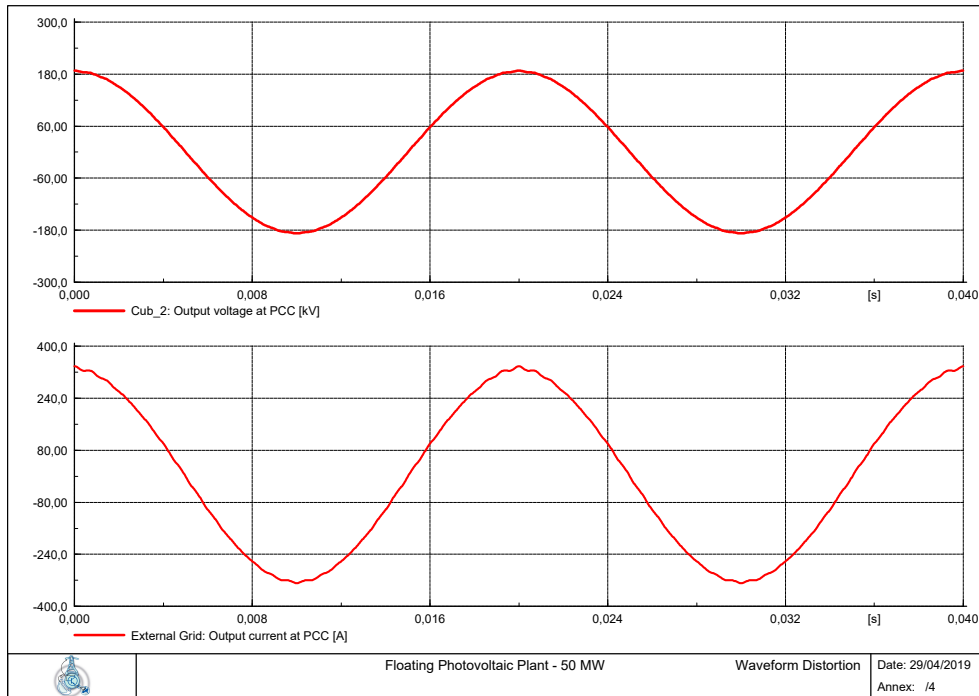
Figure 3-11: Main output waveforms at PCC. Top: Output voltage. Bottom: Output current

The bottom curve in figure 3-11, represents the current injected into the grid. In this case, the harmonic currents coming from the inverters generate slight disturbances during the peak values.

3.7   Phase Unbalance

The maximum negative phase sequence component of the phase voltage of the power system should remain below 1 % as prescribed in section 2.2 of the present document. As can be seen in figure 3-12, the negative sequence voltage (u2) is considered negligible.

```
Grid\PCC Client.ElmTerm:
  m:u2              = 0,           p.u.   (Negative Sequence Voltage)
  m:Z               = 5,589926     Ohm    (Network Impedance, Magnitude)
  m:phiz            = 84,28326     deg    (Network Impedance, Angle)
```

Figure 3-12: Negative sequence voltage u2, at PCC

Therefore, from the power quality assessment, it can be concluded that the FPV plant does not introduce abnormal waveforms and is in alignment with the energy quality requirements stated in section 2.2. Additionally, it also complies with the energy quality requirements from [19]. Consequently, it is not necessary the design of harmonic filters.

Chapter 4

Dynamic modelling of a PV inverter

This chapter presents an introduction of how to model dynamically a PV inverter in DigSILENT PowerFactory. Each inverter is independently modelled depending on the project conditions. Therefore, the modelling procedure is made following the steps indicated by the inverter's manufacturer.

4.1 Dynamic Model Overview

In DigSILENT PowerFactory, the dynamic model of a solar inverter is composed by two different parts [27]:

1. Static generator (for grid studies) or DC current source + PWM converter (for detailed studies)

2. DSL[1] model for the inverter controller

The dynamic model consists on several "slots" connected in different configurations according to the model. The number of the slots and its configuration is independent of the inverter's manufacturer and project conditions. These connections comprises the so called "*inverter's frame*".

---

[1]DSL stands for DigSILENT Simulation Language

The corresponding frame for the inverter model FS3510K is presented in figure 4-1. The frame contains the general arrangement of the dynamic model and its slots composition. Some of these slots are PowerFactory built-in models as electrical measurement systems or current sources and the other slots are DSL user-defined models, which generally represents the control of the inverters and the Phase-Locked Loop (PLL) used for grid synchronization.
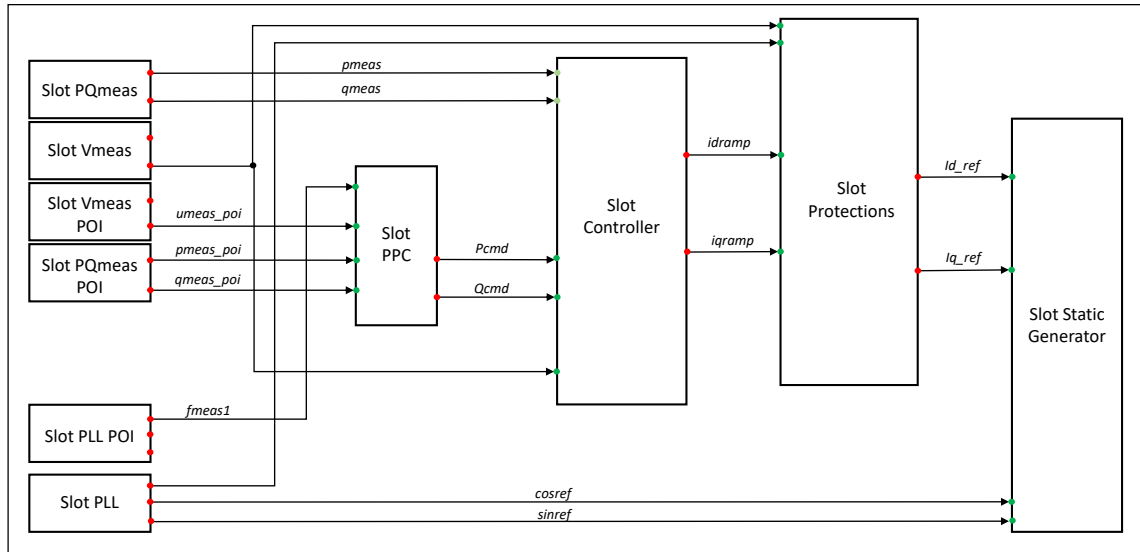
Figure 4-1: HEMK 660V FS3510K inverter's frame

According to figure 4-1, the dynamic model of the HEMK 660V FS3510K inverter is composed by the following slots:

PQ Meas Measures the output power in pu

Vmeas Measures the inverter output voltage in pu

PQmeas POI Measures the power at the point of interconnection in pu

Vmeas POI Measures the voltage at the point of interconnection in pu

PLL Allows the grid synchronization

PLL POI Measures the grid frequency at the point of interconnection

Static Generator Contains the electrical data of the inverters

Controller Includes the inverter control

Protections Includes the inverter voltage and frequency protections

PPC Contains the control algorithms for the Power Plant Controller

4.1.1   Common Model Controller

The control algorithms are include in the *slot Controller*. A general overview of the different blocks embraced in the inverter controller is represented by figure 4-2. Each block reference holds their specific dynamic control equations. The functions included
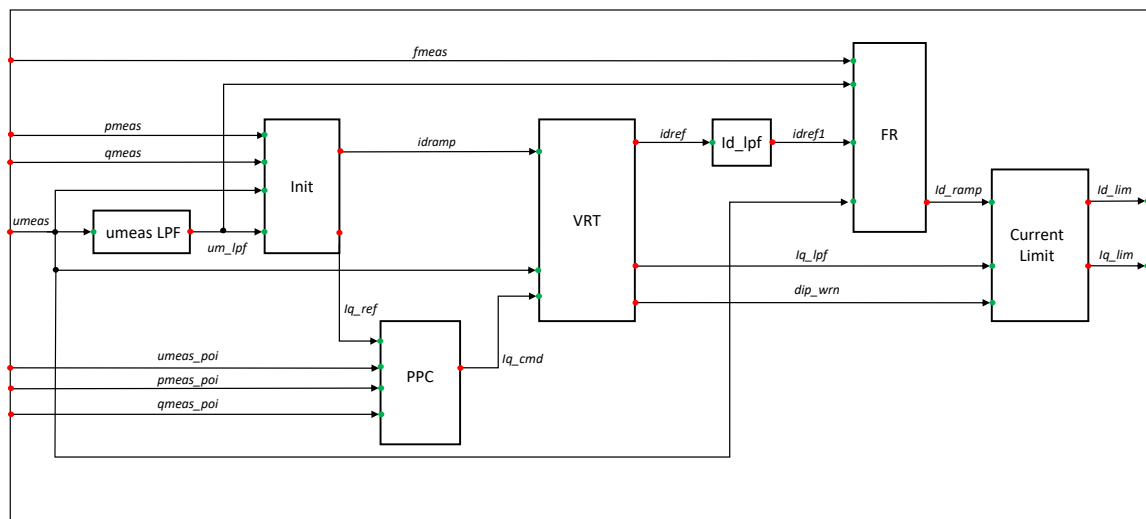
Figure 4-2: Inverter's Common Model Controller

among these block references are:

umeas LPF filters the measured inverter voltage

Init Initializes the model by calculating the initial values from the power flow

PPC Controls the voltage, active and reactive power at PCC and generates the reactive current command

VRT Includes the voltage-ride-through (VRT) control equations

id_lpf Low-pass filter for active current

63

FR Contains the equations for frequency response variations

Current_Limits Controls the current limits depending on the PQ priority

The inverter controller block diagram is shown in figure 4-3. Its response will depend on the power plant controller (PPC) status. If it is enabled (PPC = 1) then, the inputs to the controller are the active and reactive power commands (P_{CMD}, Q_{CMD}) calculated internally by the PPC. On the other hand, when is disabled (PPC = 0), the inverters are the ones who will generate the power references. There are two
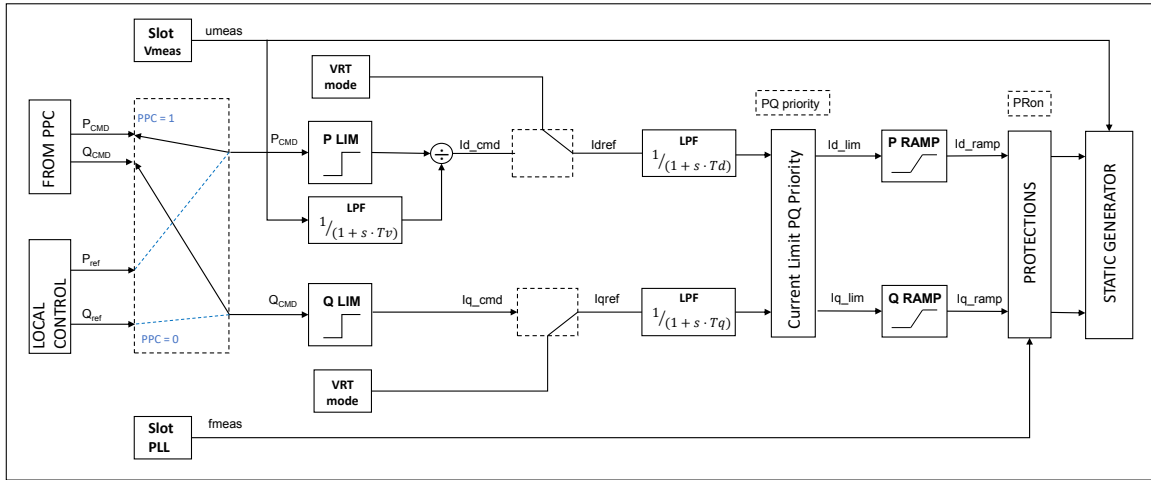
Figure 4-3: Controller block diagram

Voltage-Ride-Through (VRT) blocks that will detect an over-voltage or low-voltage situation. These blocks are responsible of helping the grid voltage to recover the steady state values after a voltage disturbance. The inverters will inject reactive current during a LVRT to increase the voltage at the external grid. On the other side, during an OVRT, the inverters will absorb reactive current to support the grid voltage. The active and reactive current references, I_d^{ref} and I_q^{ref} respectively, are filtered to avoid undesired frequency components and external noise that could be present from the measurement devices. The blocks 'P RAMP' and 'Q RAMP' will control the ramp rates of the current magnitudes to adjust it to the desired control response. Finally, the controller will send the active and reactive current orders to the static generators, which in this case are the inverters.

4.1.2 Common Model Protections

Similar to the Common Model Controller, the inverter's Protections Model is presented in figure 4-4. The block references included in this model are in charge of detecting any voltage or frequency deviation out of the defined limits. As an example, if an over-voltage is detected at the inverter's terminal over its operating limit, the voltage flag ($flagV$) is activated and the corresponding protection trips.
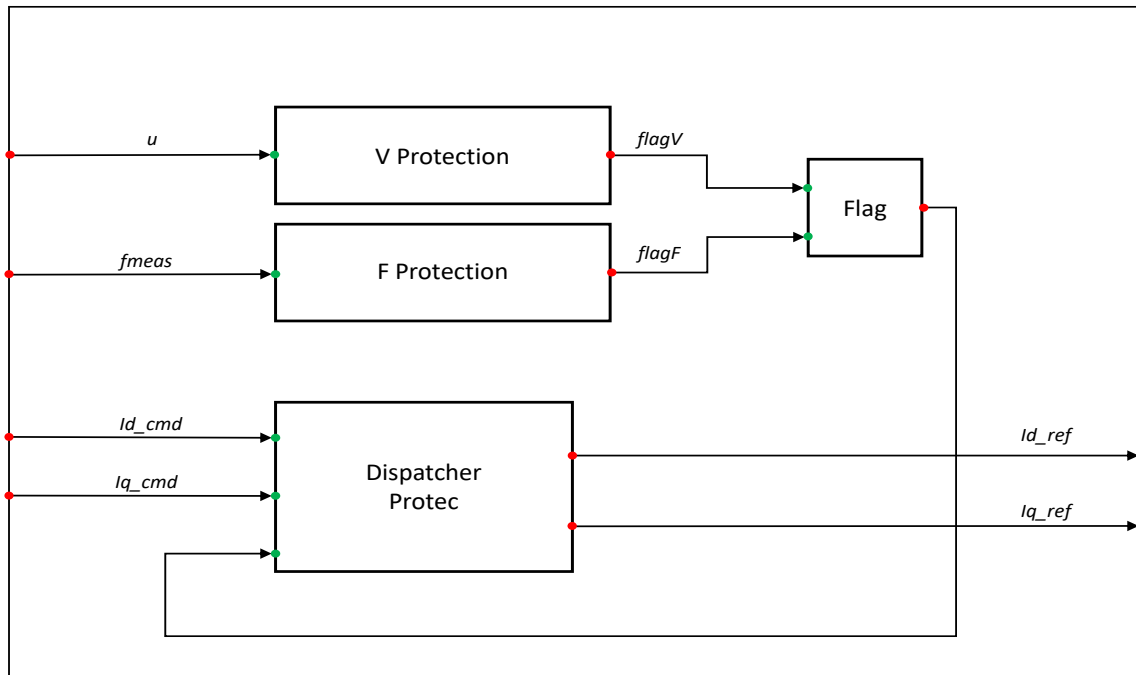
Figure 4-4: Inverter's Common Model Protections

The description of each block reference is as follows:

V Protection Includes the overvoltage and low-voltage protections

F Protection Includes the frequency protections

Dispatcher_Protec Sets currents references to 0 when a protection is activated

4.1.3 Power Plant Controller

The other user-defined block is the *slot PPC*, in which the Power Plant Controller algorithms are included. The PPC can be modelled to operate with different power reactive control modes at the point of common coupling:

1. Voltage control

2. Reactive power control

3. Power Factor control

that are selected depending on the operating requirements demanded by the TSO.
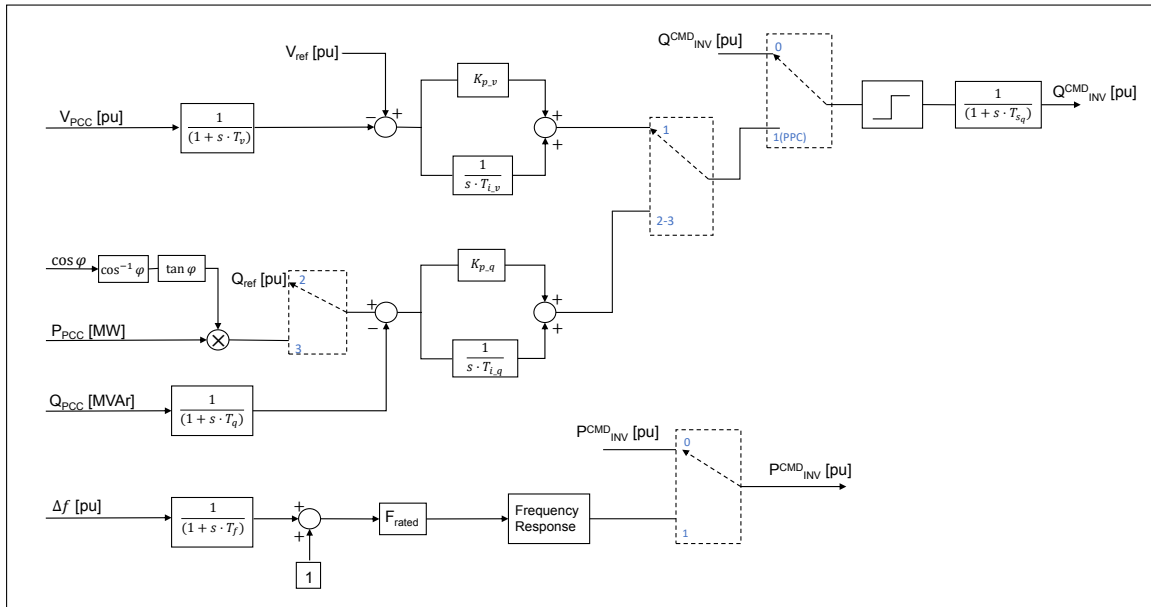
Figure 4-5: Power Plant Controller block diagram

The PPC block diagram is exposed in figure 4-5. The outputs are the active and reactive power commands for the inverter, expressed in per unit values. For the reactive power calculation, Q_{INV}^{CMD}, the algorithm depends on the reactive power control mode. The inputs could be the measured voltage at PCC (V_{PCC}), the reference power factor and active power at PCC (cos ϕ, P_{PCC}) or the reactive power at PCC (Q_{PCC}). Additionally, there is a fourth option in which the PPC is disabled. In this case, the inverter's reactive power command are the desired values entered in the model.

When the *PCC Voltage Control (V_{PCC})* is enabled, this control will try to support the controlling the voltage at PCC by injecting reactive power (capacitive) to increase V_{PCC}, or consuming reactive power (inductive) to decrease V_{PCC}. This control is achieved by means of a PI controller whose parameters depends on the external grid characteristics, in special, the short-circuit ratio. The gains of this controller are set in Appendix B.

The *reactive power control (Q_{PCC})* is based on a close loop control, measuring the reactive power at PCC. This control is also done by means of a PI controller. The reactive power control can be done by keeping it constant at a specified value or it can be controlled as function of the voltage, according to a specified droop. In this second control mode, an additional dead band can be included as shown in figure 4-6. While the reference voltage is within the dead band, the reactive power is kept constant
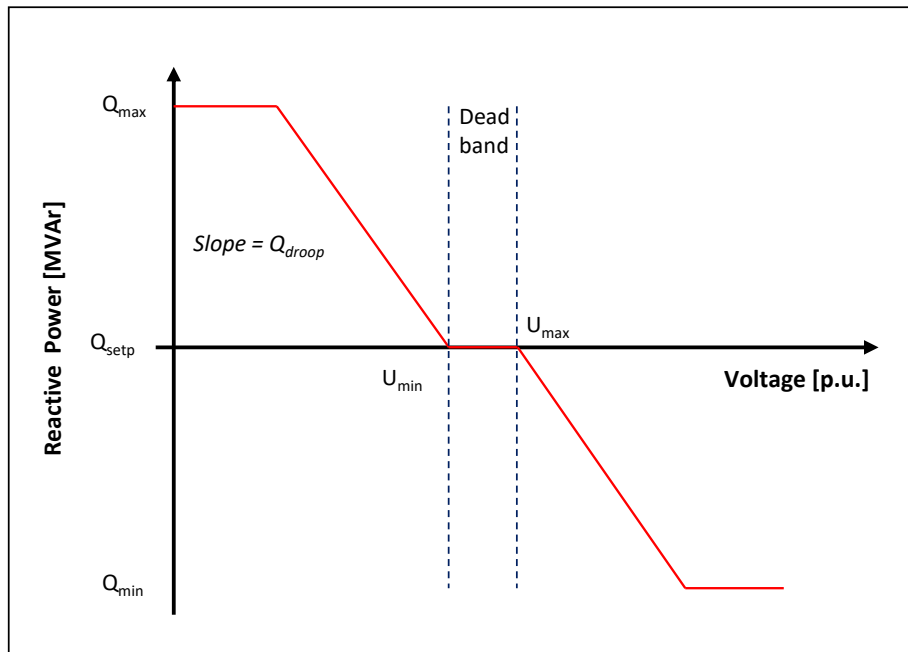
Figure 4-6: Reactive power control: Q(V) - characteristic

The last control option is the *Power Factor Control* which also is based on a close loop control, measuring the power factor and active power at PCC. The gains of the

corresponding PI controller are included in Appendix B. There exists two control modes of power factor: constant power factor an cosphi(P)-characteristic. The first one keeps the power factor constant at the specified value, whereas the cosphi(P)-characteristic follows a specified profile as the one shown in figure 4-7. In this case, the controlled power factor is determined from the characteristics curve for a certain power flow.
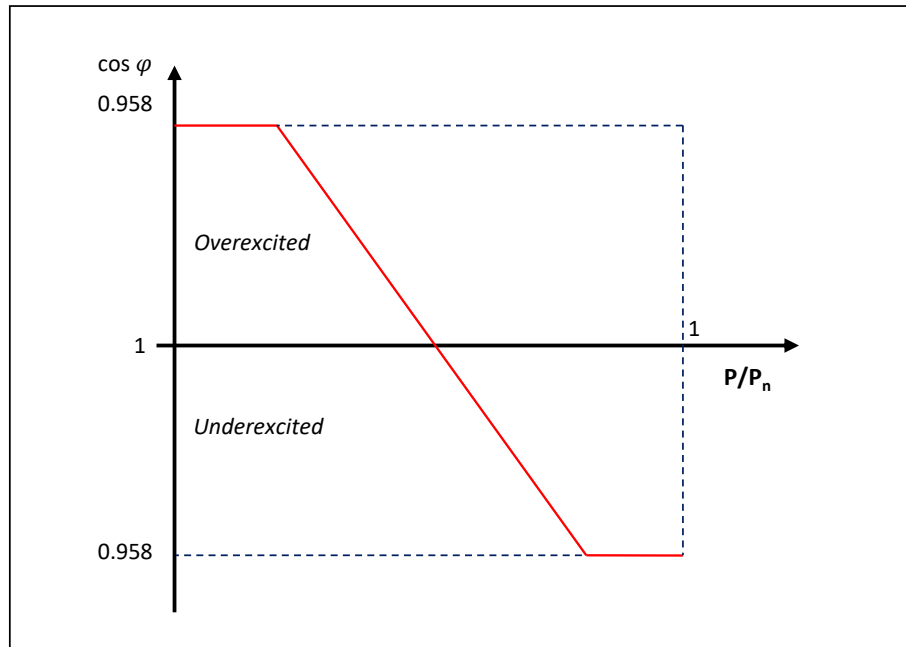
Figure 4-7: Power Factor control mode: cosphi(P) - characteristic

At the same time, when the PPC is enabled, it will calculate the active power command for the inverters from the frequency variation (Δf) measured at the point of common coupling. The function of the 'Frequency Response' block is to determine the amount of power needed to compensate such frequency variation. Similar to the reactive power control, if the PPC is disabled then, the inverters active power are the ones entered manually.

The model parameterization of the inverter controller, protections and the PPC is included in Annex B.

Chapter 5

Transient State Assessment

5.1 FPV Plant Dynamic Model

When modelling a renewable generation plant for dynamic studies, i.e. fault ride through, the level of detail in relation with the number of modules and inverters to be lumped in an equivalent machine, along with its ratings, the number of step-up transformers, equivalent low voltage and medium voltage collector circuits has to be determined.

In order to simplify the study, a single-equivalent inverter with its associated step-up transformer has been used to model dynamically the whole Floating Photovoltaic plant. To obtain this representation, it has been followed the reference published by Western Electricity Coordinating Council (WECC) [24], which is generally used as a guideline in the industry for simulating dynamic behaviour of photovoltaic plants.
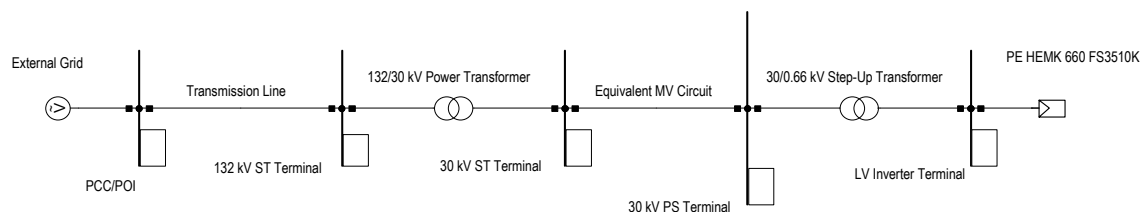
Figure 5-1: Equivalent FPV plant model for dynamic studies

To model a plant with N lumped inverters in PowerFactory, an equivalent static

69

generator is modelled with the rating of a single inverter multiplied by the total number of inverters (N). The same method is applied for the equivalent step-up transformers of the power stations. Additionally, the external grid is substituted by an AC voltage source element. Therefore, the equivalent single-line diagram used for the dynamic studies is presented in figure 5-1.

5.2 Active Power Curtailment

The FPV plant will incorporate a SCADA system responsible of sending orders to the plant controller. This section will simulate an external command received by the plant from the SCADA, derating the contracted active power output of the facility to manage the corresponding curtailment.

Table 5.1 gathers several successive active power curtailments that are going to be studied, considering that the plant is exporting 50 MW.

Table 5.1: Active power curtailment sequences

Curtailment Order (pu)		Time Event
0.85791582	49 MW @PCC	t = 5 s
0.84029362	48 MW @PCC	t = 7 s
0.82302894	47 MW @PCC	t = 9 s
0.84029362	48 MW @PCC	t = 15
0.85791582	49 MW @PCC	t = 17 s
0.87603306	50 MW @PCC	t = 19 s

In certain operating conditions, to meet with Ramp Rate requirements, a smooth transition is necessary by means of controlled steps. Therefore, to analyze the FPV plant Ramp Rate performance, two different scenarios have been proposed.

The first one, represented in figure 5-2, collects several power curtailments ensuring a smooth step-down and step-up transition of 1 MW/s from one output level to another. It can be highlighted that the output active power follows satisfactorily the orders given by the inverters.

70

Figure 5-2: Active power curtailment events with Ramp Rate of 1 MW/s
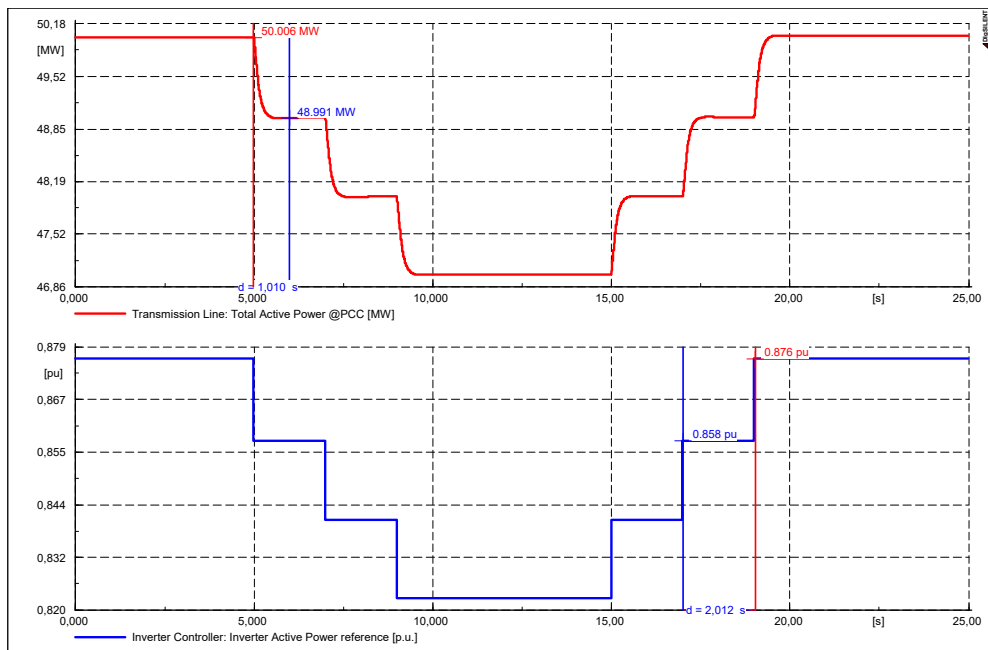
Figure 5-3: Active power curtailment events with Ramp Rate of 0.5 MW/s

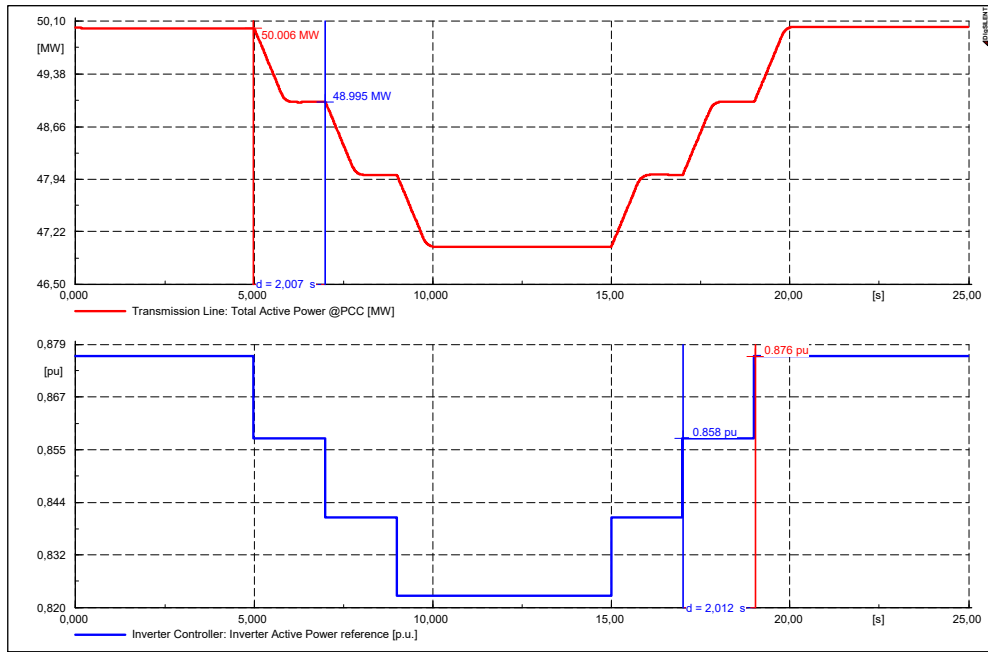Similarly, the output active power from figure 5-3 follows the inverter power commands. However, it can be noticed that in this case, the smooth transition between one power level to the next one is faster. In this case, the Ramp Rate is set to 1 MW/s.

Therefore, when the FPV plant receives orders from the SCADA system to make active power variations, the plant is able to carry out these with smooth transitions and at different ramp rates in agreement with the European grid code requirements.

5.3 Reactive Power Control

This section shows the control of the reactive power at the PCC. In this case, it is necessary to define a *Station Controller* in the PowerFactory model in order to manage the reactive power variations. Therefore, the station controller will be responsible of controlling the reactive power. Nonetheless, it is also possible to control the voltage at PCC by the station controller.

Table 5.2: PPC reactive power reference variations

Reactive Power Control					
Time (s)	Q_{ref}**(MVAr)**	P_{ref}**(MW)**	**Time (s)**	Q_{ref}**(MVAr)**	P_{ref}**(MW)**
$t_1 = 5$	5	50	$t_7 = 80$	0	35
$t_2 = 20$	14.96	50	$t_8 = 95$	20	35
$t_3 = 35$	0	50	$t_9 = 110$	0	35
$t_4 = 50$	-5	50	$t_{10} = 125$	-20	35
$t_5 = 65$	-14.96	50	$t_{11} = 140$	-20	50
$t_6 = 75$	-14.96	35	$t_{11} = 140$	0	50

The different events considered are shown in Table 5.2, which corresponds to the simulations results presented in figure 5-4. The top plot represents the voltage magnitude at PCC. It can be observed that follows the same waveform variation than the reactive power, included in the bottom plot. The PPC sends the corresponding reactive power commands represented in Table 5.2. The inverter's control is able to

manage this power variation in a smoothly transition without overshoot or oscillations. At t = 75 s, a reduction in the active power is desired which is also managed by the plant's control. When the FPV plant is exporting below its maximum power
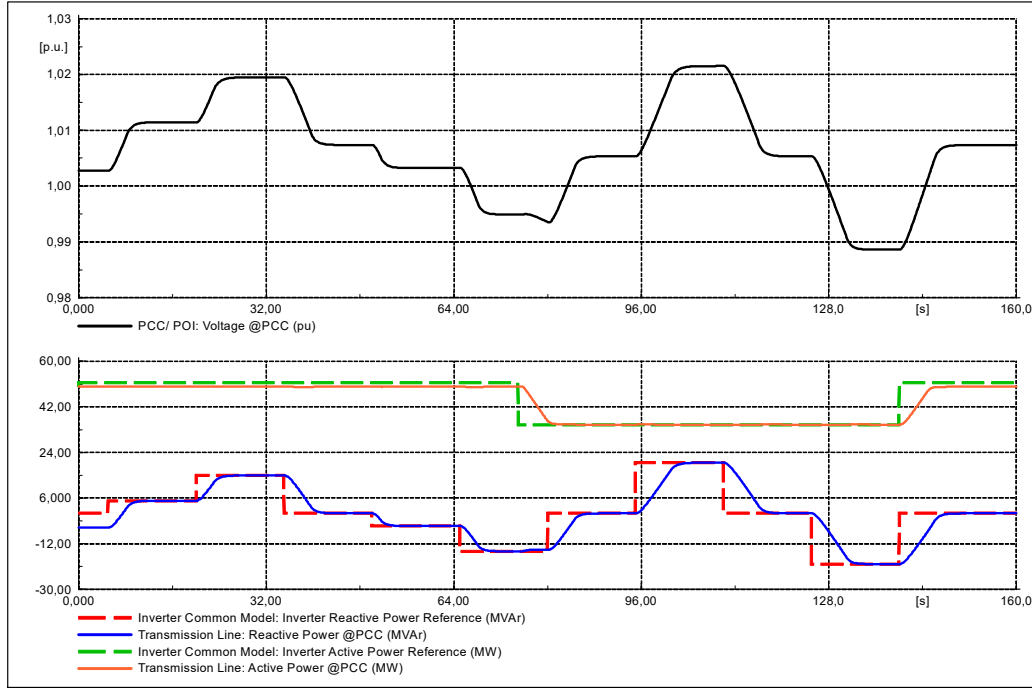
Figure 5-4: PPC reactive power control at PCC. In top figure: V_{PCC} (pu). Bottom figure includes: Q_{inv}^{cmd} (MVAr), Q_{PCC} (MVAr), P_{inv}^{cmd} (MW), P_{PCC} (MW)

then, the TSO can require the plant to inject or absorb more reactive power. This scenario is analyzed at t = 95s and t = 125 s. It is observed that the dynamics of the FPV plant are able to follow smoothly different reactive power references.

5.4   Power Factor Control

This section presents the power factor control resulting from the power flow through the PCC. The PPC calculates a reactive power set-point from the power factor and the measured current active power. Hence, the reactive power is controlled by the PPC to the new set-point at the PCC. Figure 5-5 shows how the PCC is able to regulate the reactive power control according to different power factor set-points. The first variations correspond to most demanding operating conditions: exporting

Table 5.3: PPC power factor set-points variations

Power Factor Control					
Time (s)	PF_{ref}	P_{ref}**(MW)**	**Time (s)**	PF_{ref}	P_{ref}**(MW)**
$t_1 = 10$	-0.958	50	$t_7 = 105$	1	40
$t_2 = 30$	0.958	50	$t_8 = 110$	-0.94	40
$t_3 = 50$	-0.9805	50	$t_9 = 115$	-0.94	30
$t_4 = 70$	0.9805	50	$t_{10} = 12$	0.90	30
$t_5 = 90$	-0.9889	50	$t_{11} = 150$	-0.90	30
$t_6 = 100$	1	50			

maximum active power and power factor of 0.958 leading/lagging. Both conditions are analyzed, being the FPV able to stand such operating variations. Other power factor set-points are considered, reflected in Table 5.3. Additionally, an active power reduction to 30 MW is analyzed, reducing the power factor set-point within the limits of figure 2-3.

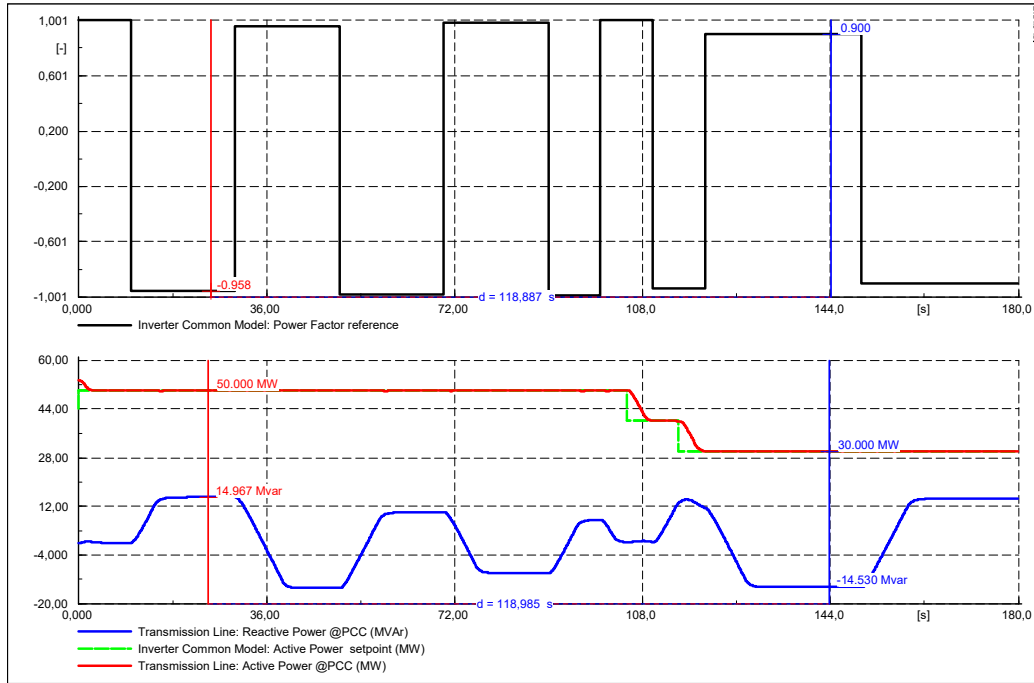Figure 5-5: PPC Power factor control. Top figure: PF reference. Bottom figure: Q_{PCC} (MVAr), P_{inv}^{ref} (MW), P_{PCC} (MW)

5.5   Voltage Droop Control

Although is not a requirement, the PPC is capable of controlling the voltage at PCC with a droop control. Hence, the PPC calculates a reactive power set-point from a built-in Q-U characteristic curve. With this control mode, the PPC manages the reactive power at PCC when the grid voltage varies within the operating limits.

Table 5.4: Voltage command values at PCC

Voltage Droop Control			
Time (s)	V_{PCC}(pu)	Time (s)	V_{PCC}(pu)
$t_1 = 10$	1.05	$t_8 = 105$	0.975
$t_2 = 20$	1.035	$t_9 = 110$	1
$t_3 = 30$	1.01	$t_{10} = 115$	0.975
$t_4 = 40$	1	$t_{11} = 12$	1
$t_5 = 50$	0.99	$t_{12} = 150$	1.035
$t_6 = 60$	0.975	$t_{13} = 150$	1.05
$t_7 = 70$	0.95	$t_{14} = 150$	1

Similar to the reactive power control, it is needed to define a station controller in the PowerFactory model. Therefore, the Q set-point is set to zero value. A voltage dead band is considered between the voltage limits 0.99 pu and 1.01 pu. It means that during the dead band, no further reactive power variation is done.

The control performance can be analyzed in figure 5-6, which includes the voltage magnitude at PCC and the total active and reactive power from the inverters. The voltage commands through the simulation are indicated in Table 5.4. As there is no voltage control at PCC, when new orders are established, there is certain overshoot before reaching the steady state value. However, this overshoot is not significant for the FPV control. The active power generated by the inverters remains constant at 50 MW, suffering slight disturbances when the grid voltage changes.

On the other hand, the PPC manages the reactive power from the inverters as
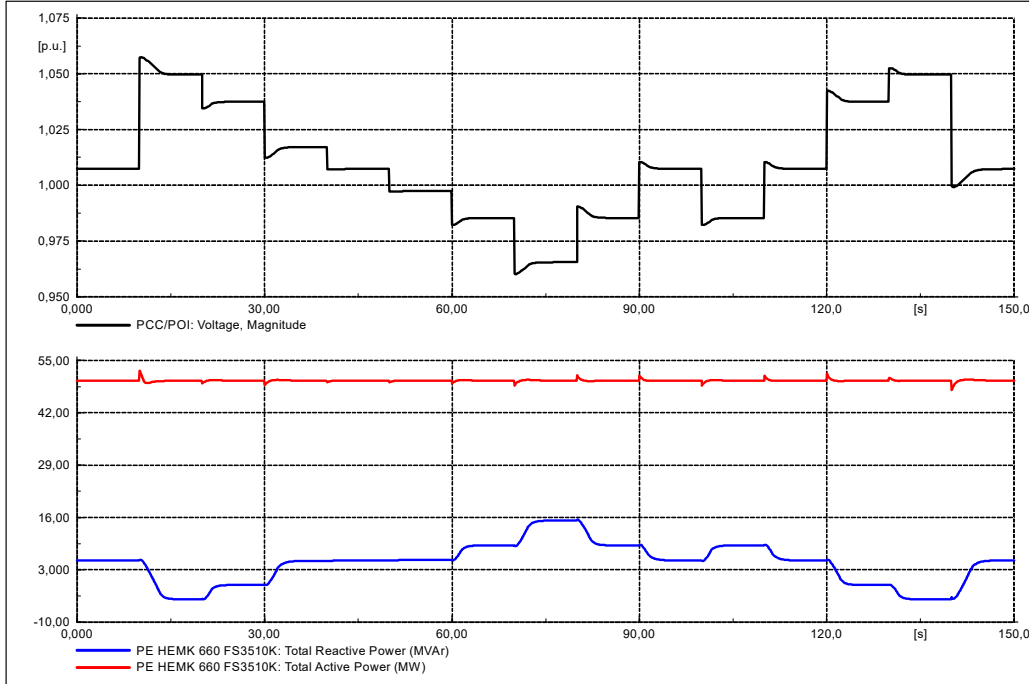
Figure 5-6: PPC voltage droop control. Top figure: PCC voltage (pu). Bottom figure: Q_{inv} (MVAr), P_{inv} (MW)

can be seen in the blue curve from figure 5-6. When the grid voltage goes over its nominal value (1 pu), the reactive power from the inverters changes from exported to absorbed. That is, in order to compensate a voltage increase, the inverters absorb reactive power. Alternatively, if voltage goes down 1 pu, the inverts inject more reactive power in the system to compensate.

The voltage droop dead band can be perceived between the time interval 30-60 seconds. According to Table 5.4, the dead band occurs inside this period and from figure 5-6, no reactive power variation is noticed as expected.

5.6   Active Power - Frequency Control

This section studies the active power - frequency control mode. Several load variations are considered at the external grid, that will cause frequency perturbations. The inverter's control should counteract by injecting more active power (in the case that frequency decreases) or reduce active power generation (when frequency increases).

The simulation time is set to 100 seconds and the reactive power control mode is set to constant reactive power. Additionally, the initial operating conditions considered are the FPV plant exporting its nominal active power with unity power factor.

Figure 5-7 shows two different study cases for active power - frequency control. In figure 5-7a, a load decrease is done in several steps. When the load is reduced, grid frequency increases. This causes that the inverter's active power control is activated, reducing its output power until restoring the power - frequency balance. As it is defined in section 2.3.1, no power control is expected until the frequency goes out the frequency regulation limits (49.8 Hz - 50.2 Hz).

It can be observed in figure 5-7a that the active power is not reduced until the grid frequency rises up to 50.2 Hz, as expected according to P.O. 12.2 requirements. Furthermore, for each load variation, the inverters control are able to achieve steady state operating condition at different frequencies. The maximum frequency reached is below 51.5 Hz. Hence, the overfrequency trip protection is not activated.

However, as defined in Table 2.3, if grid frequency goes down 47.5 Hz, or over 51.5 Hz, the FPV plant must disconnect immediately. This situation is considered in figure 5-7b. In this case, the considered load variations are more strict, causing abrupt frequency variations than in figure 5-7a. As consequence, as soon as grid frequency rises to 51.5 Hz, the inverter's protections must disconnect immediately as it does. As it is indicated in figure 5-7b, for a frequency value of 51.501 Hz, the active power is zero since the inverters are uncoupled from the grid.
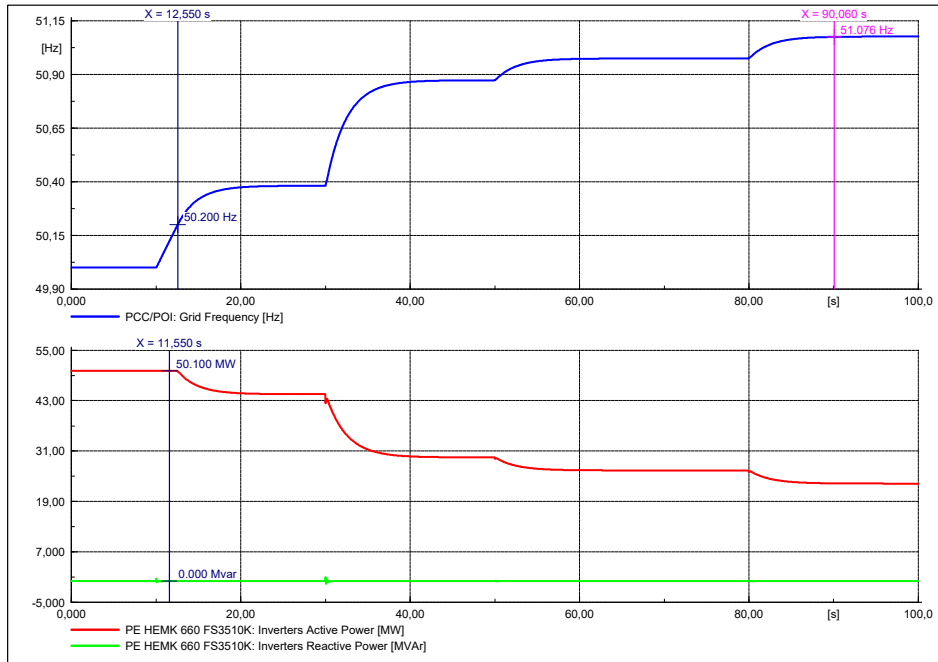
(a) Case 1: Grid frequency and inverters output active power without grid disconnection
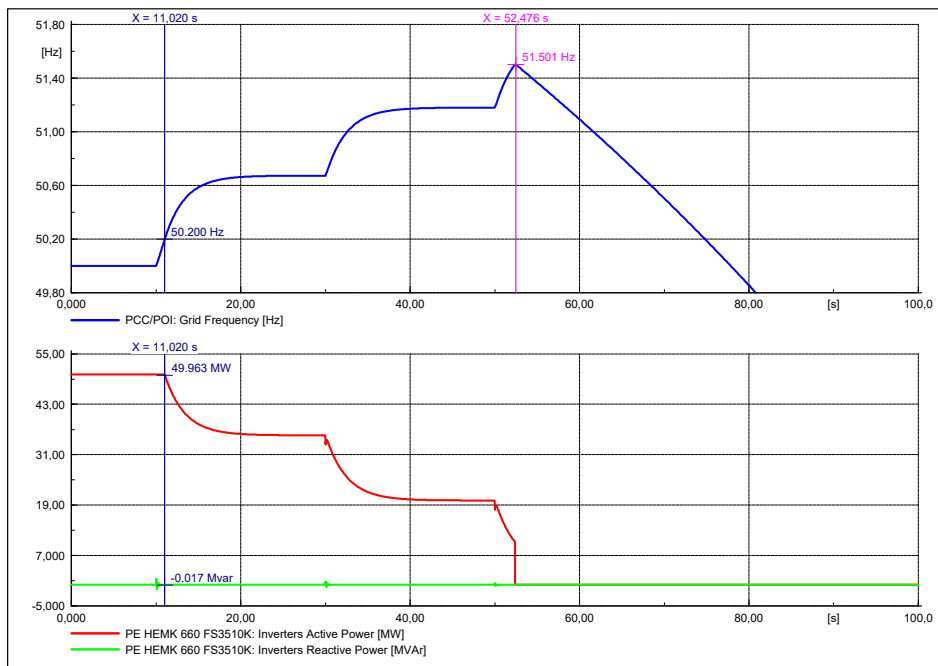
(b) Case 2: Grid frequency and inverters output active power with grid disconnection

Figure 5-7: Active power - frequency control. a) Case 1: without grid disconnection, b) Case 2: with grid disconnection

78

5.7 Active Power Reduction for Over Frequency

This section is similar to previous one. However, the difference is that in this case, frequency variations are directly given by the external grid (AC voltage source as shown in figure 5-1) and are not caused by load variations as is considered in section 5.6.

The inverters will reduce its active power at the PCC at a frequency of 50.2 Hz onward, following the dynamics established in section 2.3.1, with a maximum operating frequency of 51.5 Hz. No dead band has been considered for the control. Table 5.5 embraces the different frequency events that take place in this simulation. The simulation results are presented in figure 5-8. At the beginning, the FPV is

Table 5.5: Grid over-frequency set-point

Over-frequency Control			
Time (s)	Frequency (Hz)	Time (s)	Frequency (Hz)
$t_1 = 10$	50.15	$t_6 = 40$	50
$t_2 = 15$	50	$t_7 = 60$	51.5
$t_3 = 20$	51	$t_8 = 65$	50
$t_4 = 25$	50	$t_9 = 70$	51
$t_5 = 30$	51	$t_{10} = 75$	50

initialized from its nominal values to a steady state operating condition, exporting 50 MW and 14.96 MVAr. While the frequency does not exceed 50.2 Hz, the frequency response control is not activated as required in P.O. 12.2. However, the inverters reduce their active power when the frequency measured at the grid is 50.5 Hz at t = 20 s. Also, it can be observed that once the frequency recovers to its nominal value, the plant also recovers the operating point prior the over-frequency. The reactive power, in this case injected to the grid, suffers slight oscillations when the frequency changes, but do not suppose problems to the FPV plant's control.
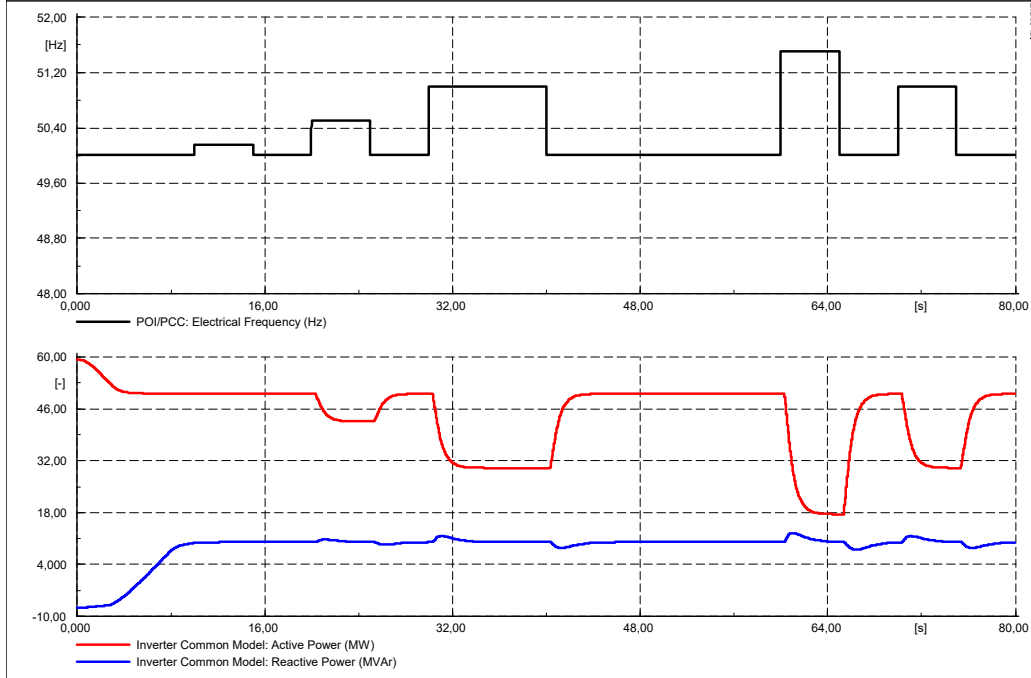
Figure 5-8: Active power reduction during over-frequencies

5.8 Voltage Ride Through Assessment

During Voltage Ride Through (VRT) event, the inverter should inject reactive current $(i_q > 0)$ or absorb it $(i_q < 0)$, depending if it is a LVRT or OVRT respectively. The inverter control response depends on the variables K_{lvrt} and K_{ovrt} [1], which represent the reactive current injection gain during under and over voltage respectively. These variables are included in the *Common Model Controller*.

As the objective of this section is to analyze the behaviour of the FPV plant against sudden voltage disturbances at the PCC, it is important to have present the robustness requirements described in section 2.5 which defines the trip points of the protections.

The inverters shall withstand such voltage conditions and bring back the FPV plant to a steady state condition with enough speed and stability.

During the following simulations, the plant has been considered coming from a steady state while it is injecting 50 MW to the grid.

---

[1]Inverter control parameters are included in Appendix B.

5.8.1 Over-voltage Ride Through (OVRT) simulations

In order to analyze the behavior of the FPV while facing overvoltage disturbances, several simulations have been developed at the PCC terminal. As the inverter model does not incorporate enough high voltage relay levels, it is necessary to set the high voltage relay levels for each simulation, despite the fact that the substation will have sufficient voltage relays and voltage levels to fully comply with the grid code. From

Table 5.6: Different OVRT cases considered in the study

	V_{ORT} [pu]	Event duration [ms]	Voltage recovery	Result
Case 1	1.21	Permanent	1.21	FPV disconnects
Case 2	1.20	400	1	FPV disconnects
Case 3	1.20	40	1	FPV remains connected
Case 4	1.15	850	1	FPV remains connected

figure 2-5, an OVRT condition is detected if the voltage at PCC exceeds V_{max}, which has been defined to be 1.15 pu. If the voltage reaches 1.20, the FPV plant must disconnect from the grid if the event duration is longer than 50 ms or should disconnect immediately in the case that the voltage rises over 1.20 pu. On the other hand, the maximum duration that the plant should be capable to operate during an OVRT event is 1000 ms, only if the voltage is 1.15 pu. Four different simulations have been carried out in order to study the OVRT plant response. The characteristics for each simulation case are given in Table 5.6.

In **case 1**, the voltage increases up to 1.21 pu at PCC. Consequently, the FPV plant protections should trip at the time that they detect that the voltage has exceeded the limits. Figures 5-9a and 5-9b show the inverters control response, disconnecting immediately from the grid as expected. This disconnection can be identified in the inverter waveforms from figure 5-9b, in which at the time the OVRT is occurred, the output current goes down to zero.
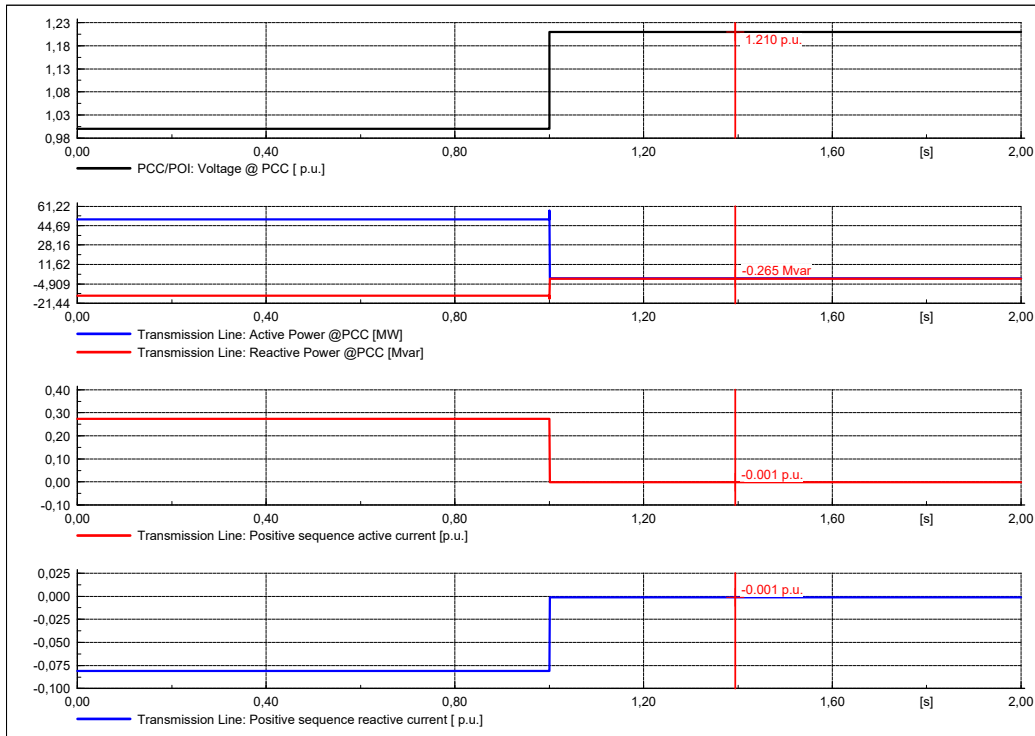
(a) Case 1 - PCC main waveforms: voltage, active and reactive power flow, active and reactive currents
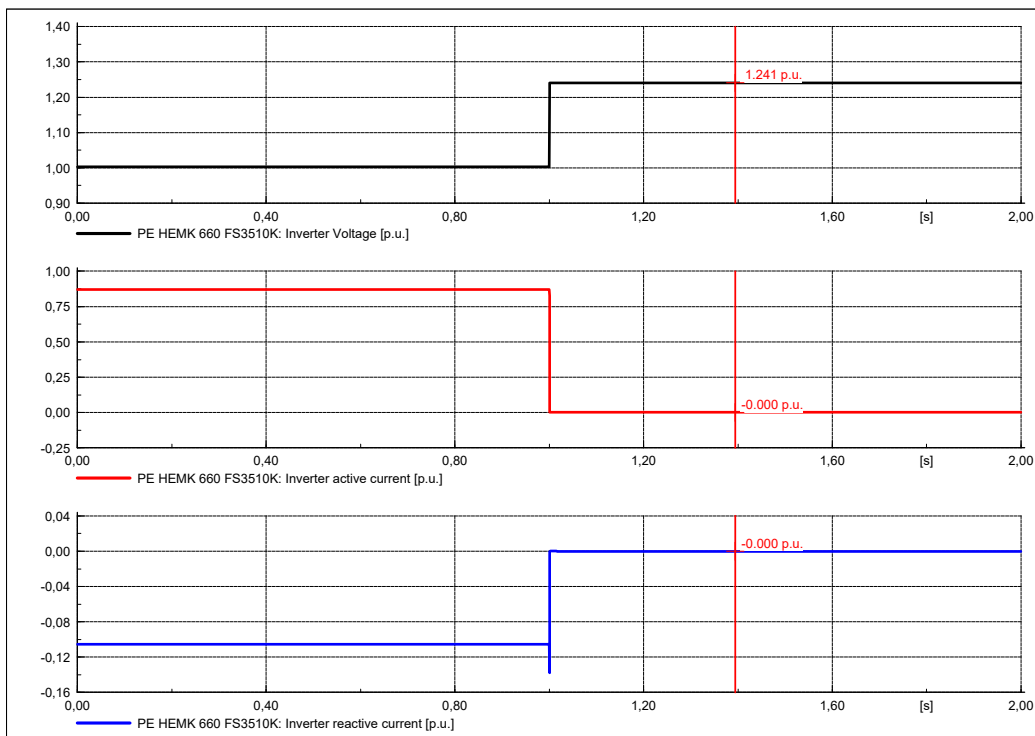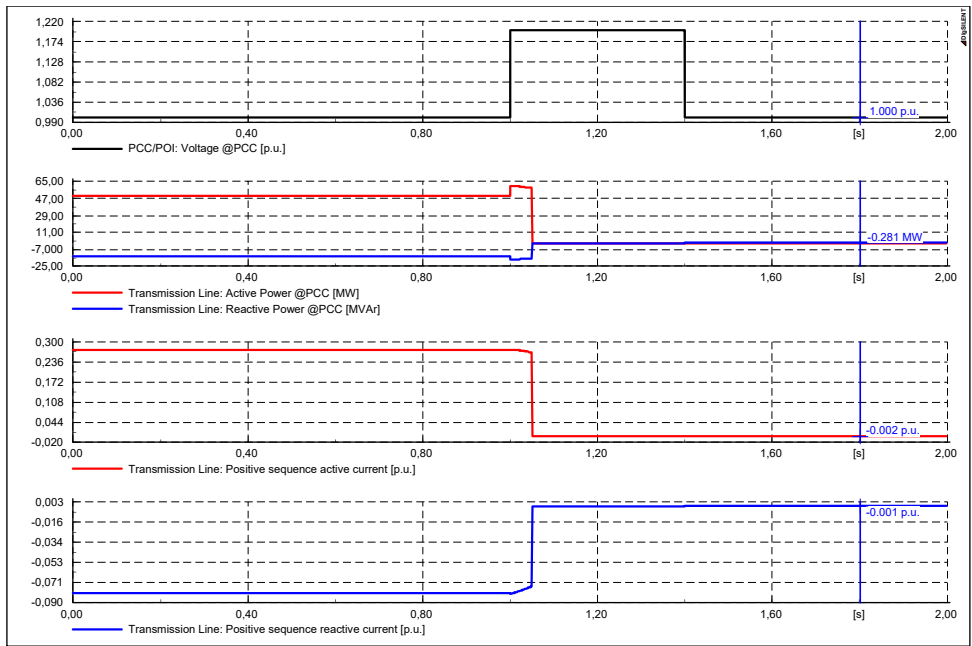

(b) Case 1 - Inverter main waveforms: voltage, active and reactive current

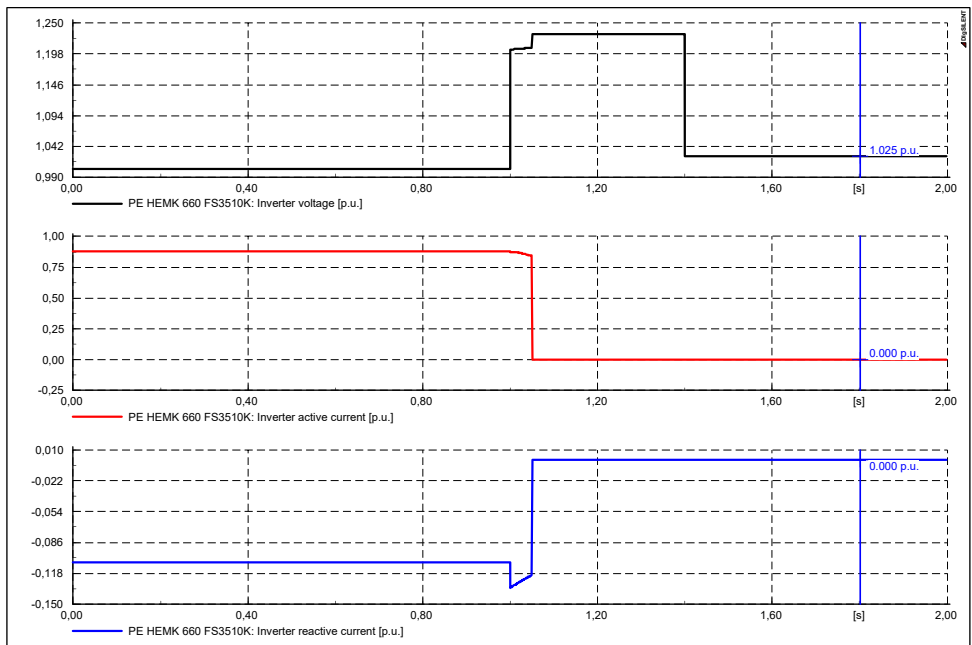Figure 5-9: Case 1 - Over voltage 1.21 pu at PCC

During **case 2**, it has been considered that the voltage rises to 1.20 pu, during 400 ms. The maximum operating duration at this voltage level for the plant is 50 ms. As result, the FPV must disconnect from the grid as it does. This is verified in figures 5-10a and 5-10b. The main waveforms at the PCC are shown in figure 5-10a, where it can be observed how the voltage rises to 1.20 pu. As consequence of this voltage increase, both active and reactive power increase in absolute value while the plant remains connected to grid. After 50 ms, the relays trip and the inverters disconnect as observed in figure 5-10b.

The same voltage level at PCC is considered in **case 3**. However, the event duration is 40 ms, which is below the maximum time allowed for the FPV to operate at this level. Hence, the FPV remains connected to the grid, recovering the steady state operating values after the OVRT event. FPV plant response can be analyzed in figures 5-11a and 5-11b. It can be observed that the power flows tend to recover their operating conditions before the OVRT is occurred. It is considered that the FPV is operating with an inductive power factor. Thus, the inverters absorb reactive current during the OVRT trying to recover the voltage level at PCC. After the disturbance is cleared, the inverters are capable to recover the nominal operating conditions.

The last OVRT event is **case 4**, in which the voltage at PCC goes up to 1.15 pu. At this voltage, the FPV plant will be capable to operate during 1000 ms. Since the disturbance is present only 850 ms then, the FPV plant must remain connected to the grid, as it does. Figure 5-12a represents the behaviour at the PCC, where in effect, the FPV plant remains connected. The inverters are capable to counteract to the overvoltage by reducing the output active power as can be observed in figure 5-12b. As the plant is considered to operate with a capacitive power factor then, during the OVRT event, the inverters also reduces their capacitive reactive current to later, recover the steady state operating conditions exporting 50 MW to the grid.

(a) Case 2: PCC main waveforms: voltage, active and reactive power flow, active and reactive currents

(b) Case 2: Inverter main waveforms: voltage, active and reactive current

Figure 5-10: Case 2 - Over voltage 1.20 pu at PCC

(a) Case 3 - PCC main waveforms: voltage, active and reactive power flow, active and reactive currents:

(b) Case 3 - Inverter main waveforms: voltage, active and reactive current

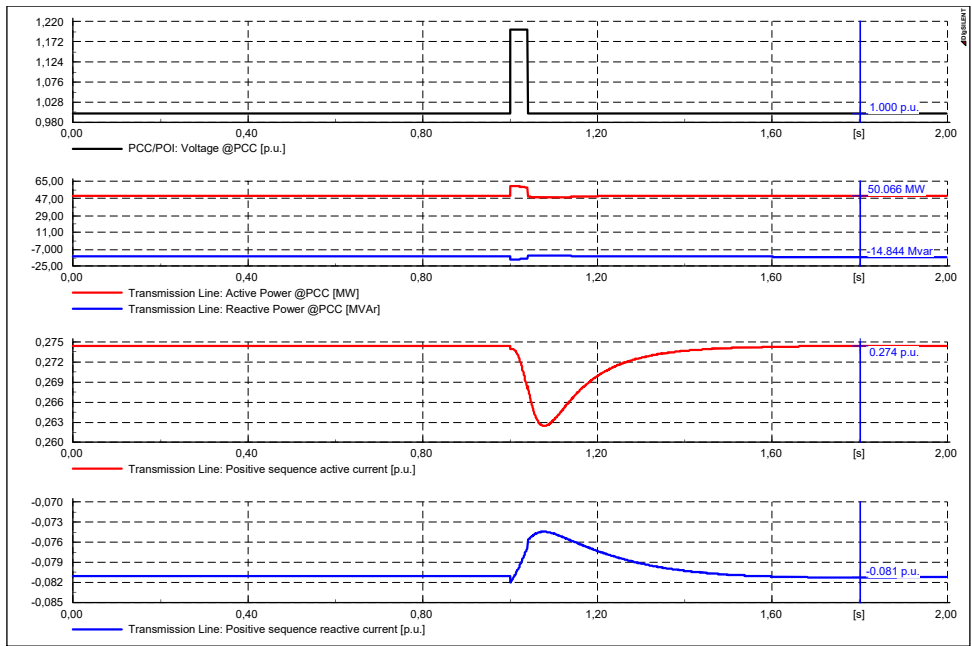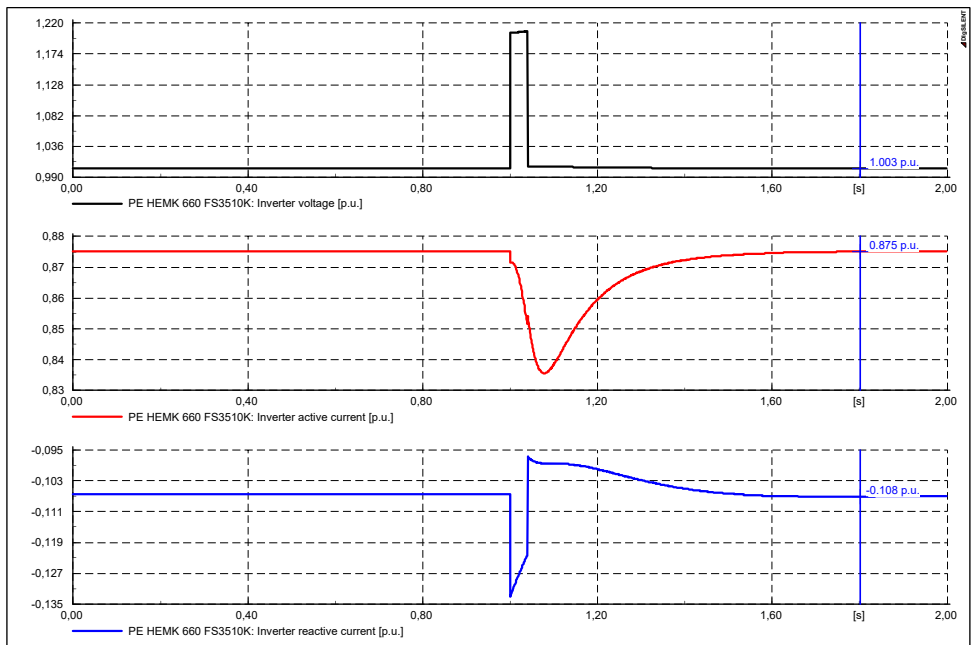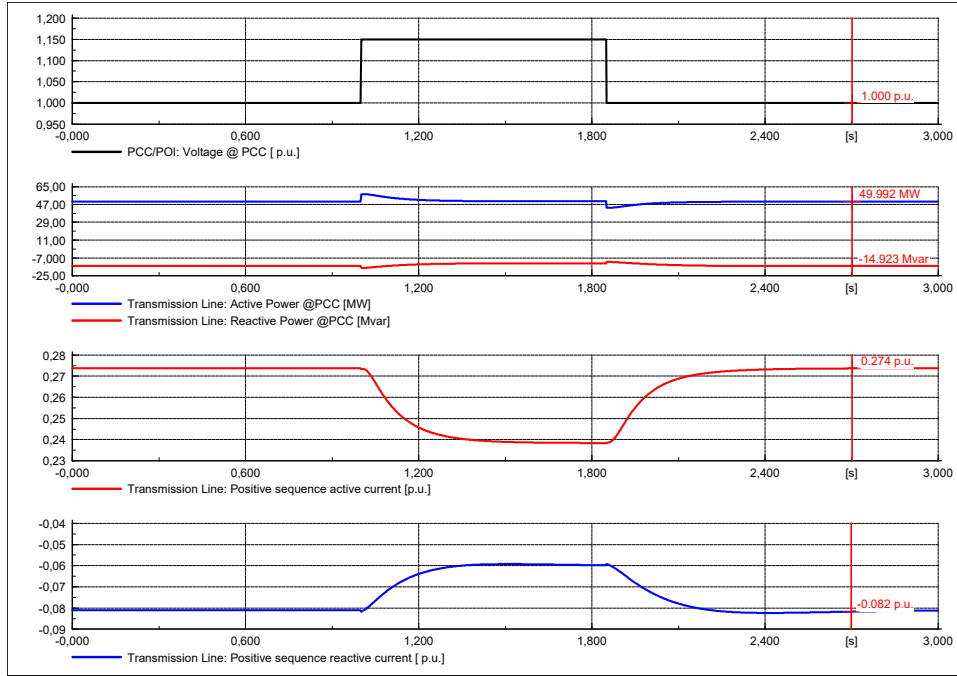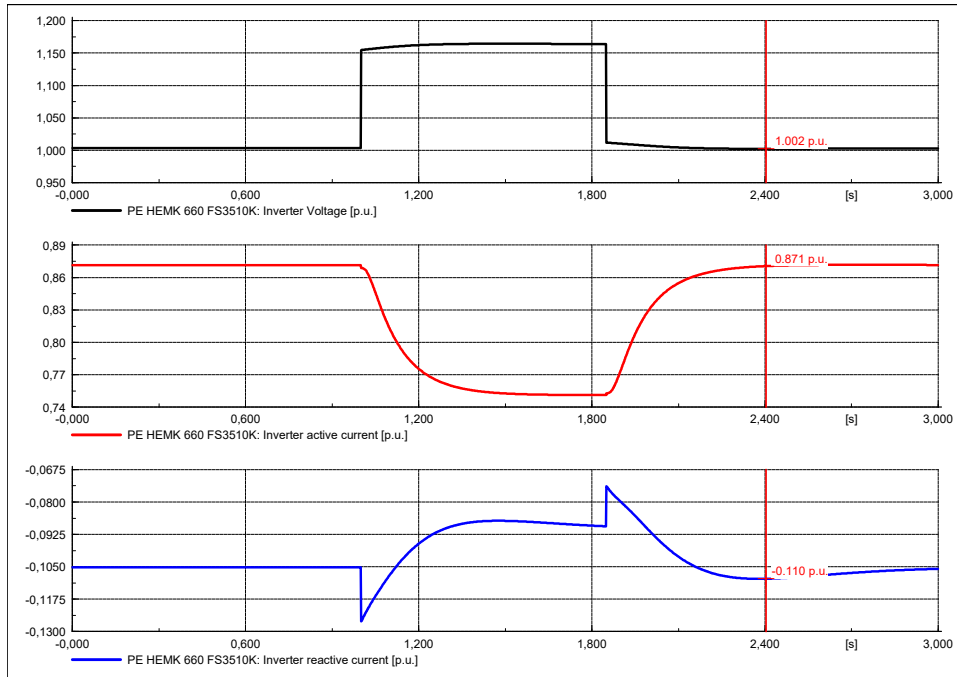Figure 5-11: Case 3 - Over voltage 1.20 pu at PCC

(a) Case 4 - PCC main waveforms: voltage, active and reactive power flow, active and reactive currents

(b) Case 4 - Inverter main waveforms: voltage, active and reactive current

Figure 5-12: Case 4 - Over voltage 1.15 pu at PCC

5.8.2 Low-voltage Ride Through (LVRT) simulations

To analyze the performance of the FPV plant against low-voltage disturbances, four different simulations have been studied at the PCC, with different conditions in accordance with the low-voltage-ride-through (LVRT) boundary of figure 2-4.

A LVRT condition is identified when the voltage level goes down 0.85 pu at the PCC. According to P.O. 12.2 conditions, if a fault is produced, generating a zero-voltage level, the plant has 150 ms to recover, otherwise it must disconnect from the grid. If the voltage level is at 0.85 pu, the plant is allowed to operating in this condition during 1.35 seconds as defined in figure 2-4. The characteristics of the different LVRT cases considered are comprised in Table 5.7. Cases 1 and 2 simulates a zero-

Table 5.7: Different LVRT cases considered in the study

	V_{LVRT} [pu]	Event duration [ms]	Voltage recovery	Result
Case 1	0.00	100	1	FPV remains connected
Case 2	0.00	300	1	FPV disconnects
Case 3	0.50	500	1	FPV remains connected
Case 4	0.50	1000	1	FPV disconnects

voltage fault with different disturbances duration. Whereas in case 1, the protections do not trip as the fault is cleared in 100 ms, in case 2 the FPV plant is disconnected at the time the LVRT exceeds the allowed length of time for this voltage level at the PCC.

Similar approach is followed in cases 3 and 4. The voltage goes down to 0.55 pu with event time periods of 500 ms and 1000 ms respectively. Since the maximum time for a 0.55 pu disturbance is calculated from the LVRT boundary of figure 2-4 to be approximately 800 ms, the FPV plant will remain connected to the grid in case 3 while it should disconnect from the grid in case 4.

During a LVRT, the inverter will inject capacitive reactive current ($i_q > 0$) in order to support the grid to recover the steady state voltage. It is important to

mention that the inverter control model has two different response modes against LVRT events, given by the expressions (5.1) and (5.2).

$$LVRT\_mode = 0 \ [I_d = 0, I_q = K \cdot V] \tag{5.1}$$

$$LVRT\_mode = 1 \ [I_d = I_d^{prev}, I_q = I_q^{prev} + K \cdot V] \tag{5.2}$$

In this thesis, LVRT_mode = 0 is considered. This means that during a LVRT event, the inverters active current will reduce to 0 and they will inject the enough reactive current to stabilize the grid voltage.

The main waveforms corresponding to the FPV plant response from **case 1** are shown in figure 5-13a, which represents the behaviour at the PCC and in figure 5-13b which presents the voltage, active current and reactive current at the inverters. As it was explained, it can be observed in this last figure how the active current output from the inverters is reduced, while all injected current is reactive, in order to help the grid to recover the voltage. Since the duration of the fault is lower than 150 ms, the plant remains connected to the grid and is capable to operate in normal conditions exporting 50 MW as seen in figure 5-13a.

On the other hand, in **case 2**, the FPV plant is disconnected as is deduced from figures 5-14a and 5-14b. The active current does not completely go to zero value as defined by ((5.1)) because of the losses through the conductors. However, after 150 ms of LVRT duration, the inverters are completely removed.

In **case 3**, a similar control response is obtained to the one in case 1, as it is observed in figures 5-15a and 5-15b. The difference is that the voltage disturbance level is at 0.55 pu, but since the duration is lower than the maximum allowed as indicated in Table 5.7, the FPV plant does not disconnect during the LVRT event.

On the other hand, the voltage level in **case 4** is the same as in previous case, but in this scenario, disturbance is expected to persists more time than the allowed one. Therefore, the protections of the plant must trip, disconnecting it from the grid, as is deduced from figures 5-16a and 5-16b.
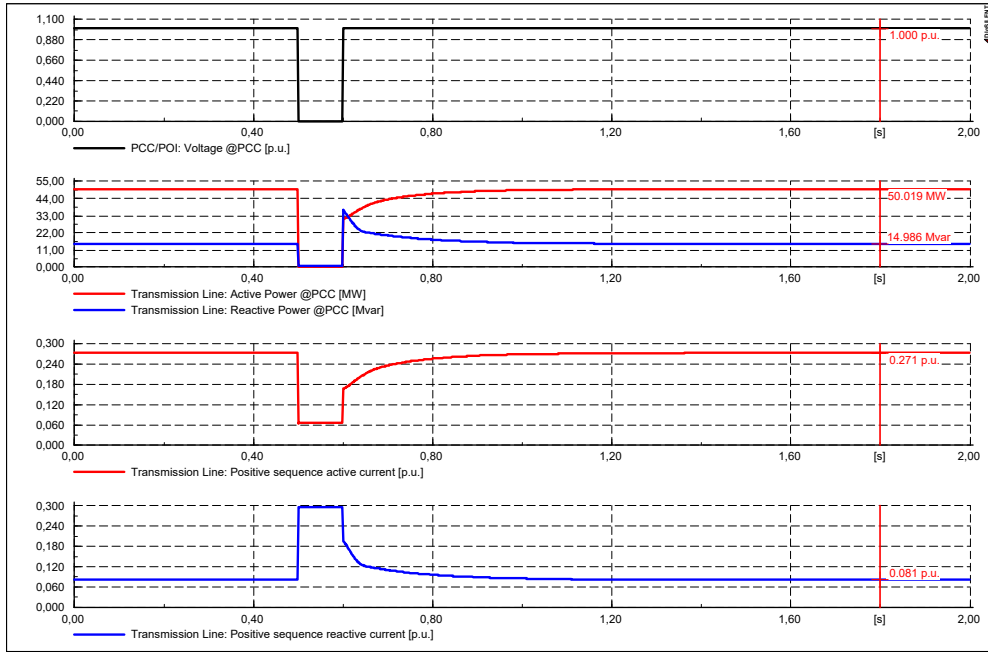
(a) Case 1 - PCC main waveforms: voltage, active and reactive power flow, active and reactive currents
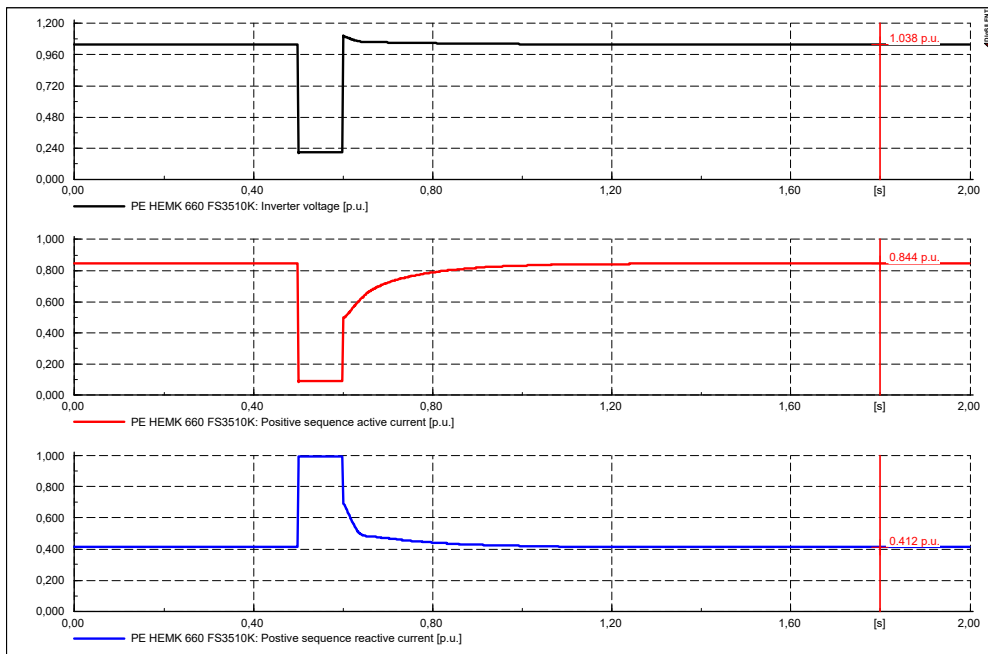
(b) Case 1 - Inverter main waveforms: voltage, active and reactive current

Figure 5-13: Case 1 - Low voltage 0.0 pu at PCC

(a) Case 2 - PCC main waveforms: voltage, active and reactive power flow, active and reactive currents

(b) Case 2 - Inverter main waveforms: voltage, active and reactive current

Figure 5-14: Case 2 - Low voltage 0.0 pu at PCC

(a) Case 3: PCC main waveforms: voltage, active and reactive power flow, active and reactive currents
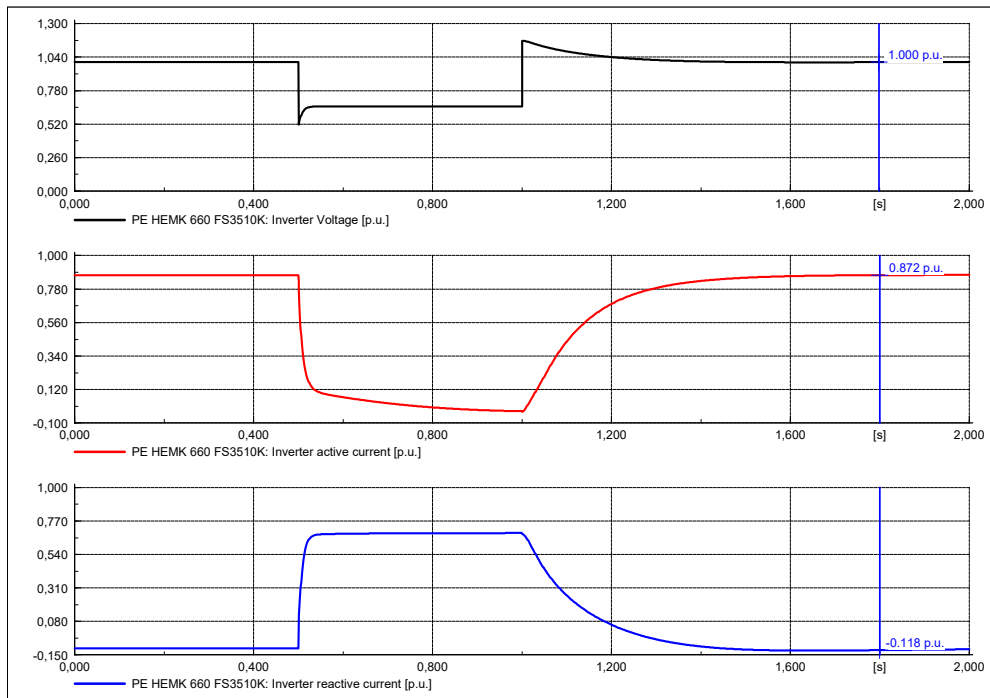
(b) Case 3: Inverter main waveforms: voltage, active and reactive current

Figure 5-15: Case 3 - Low voltage 0.50 pu at PCC
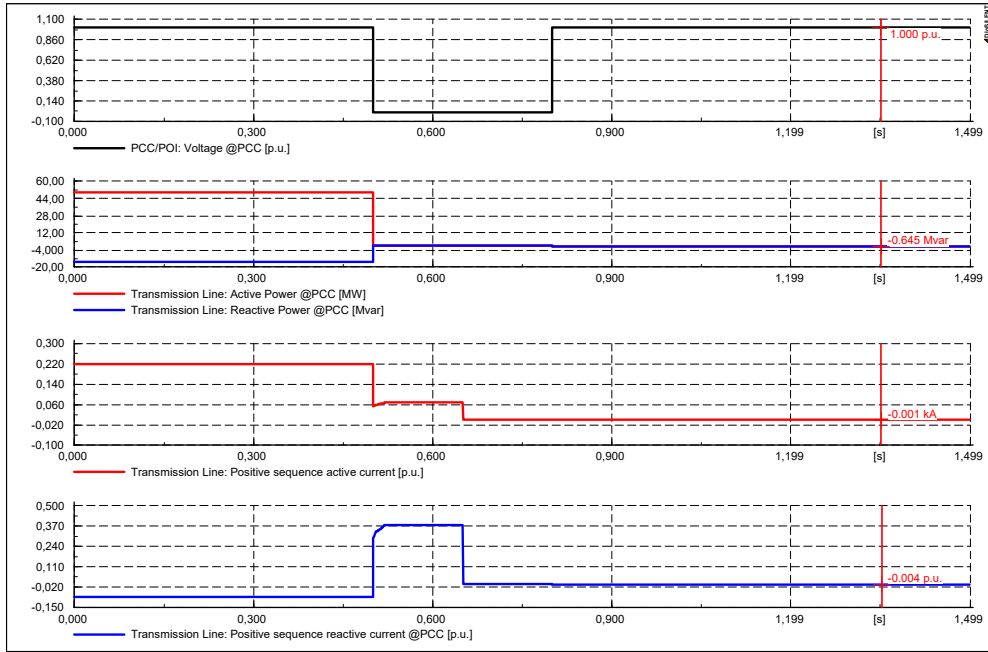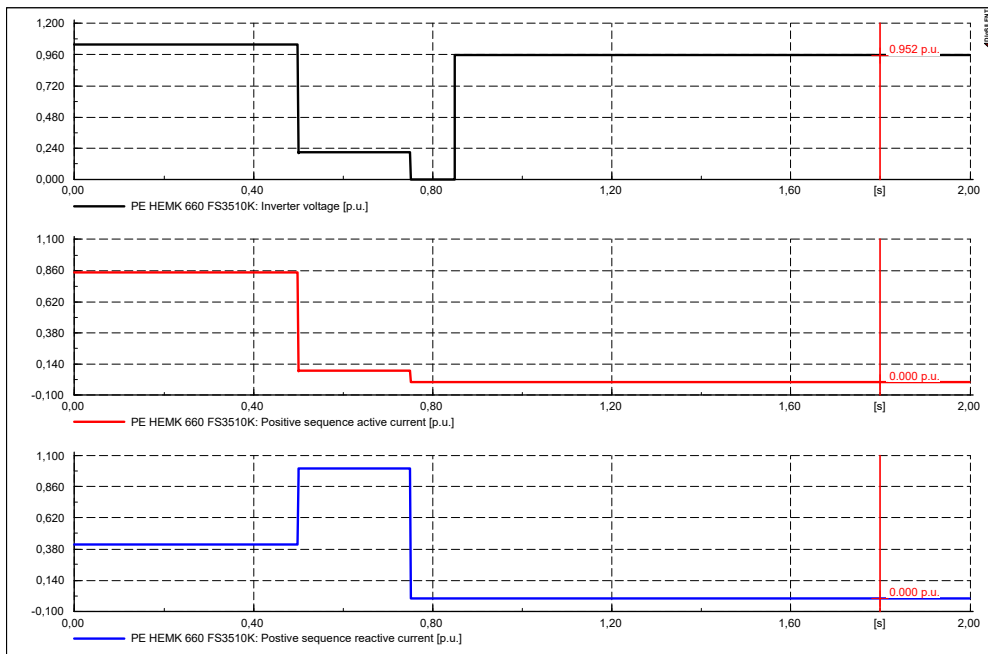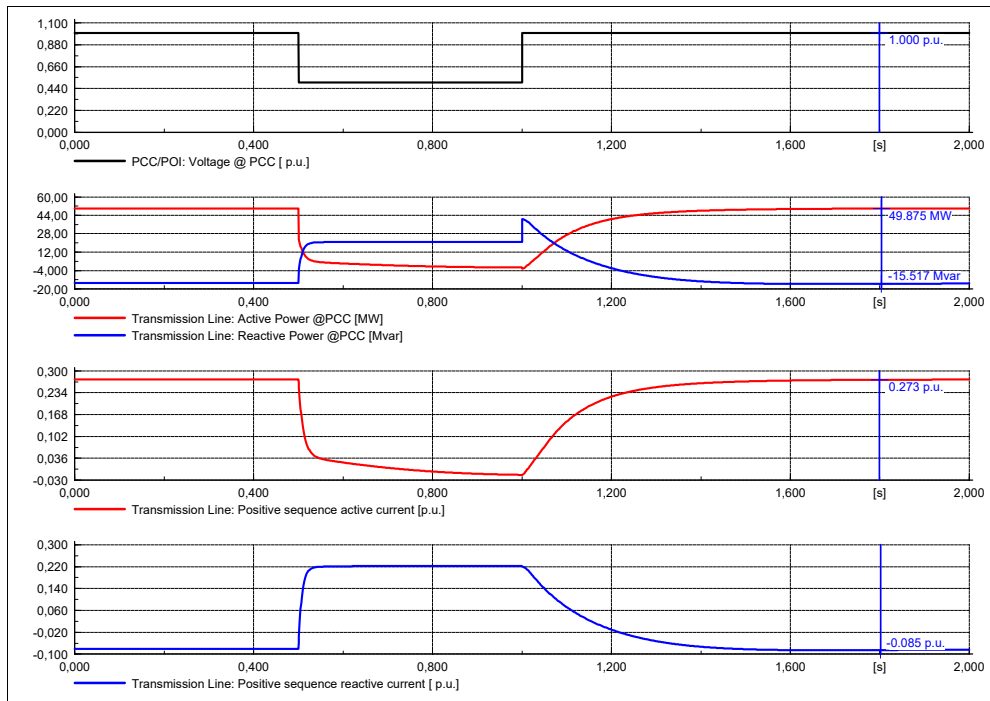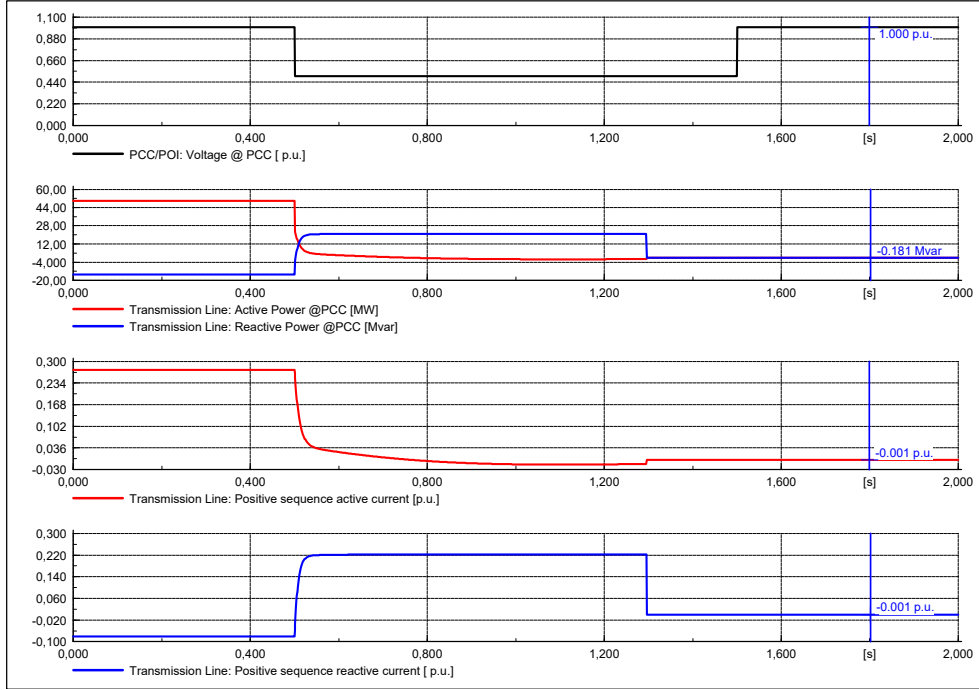
(a) Case 4 - PCC main waveforms: voltage, active and reactive power flow, active and reactive currents
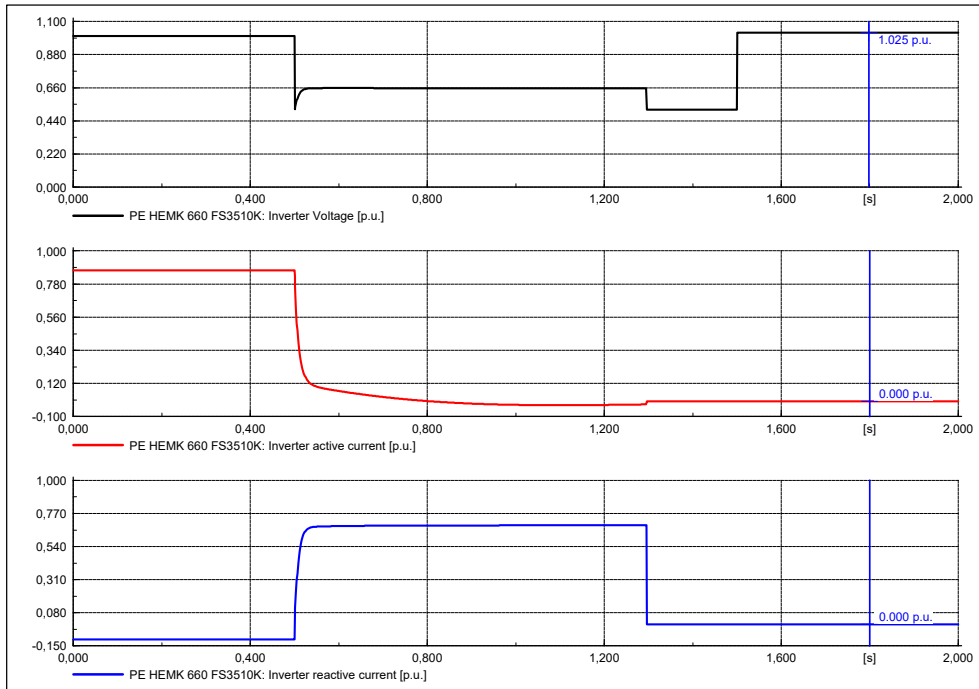
(b) Case 4 - Inverter main waveforms: voltage, active and reactive current

Figure 5-16: Case 4 - Low voltage 0.50 pu at PCC

Chapter 6

Conclusions and Future Work

6.1 Conclusions

Floating photovoltaic plants or *floatovoltaics*, are a recent technology with only 10 years of development. Nonetheless, its high potential is noticeable in the renewable energies market, with several large-scale FPV plants being deployed in the last years. A higher energy yield due to lower cell operating temperatures and the exploitation of unused water surfaces such as hydropower plant reservoirs are the main advantages of *floatovoltaics*.

The objective of the present Master Thesis was to evaluate the grid impact of a 50 MW Floating Photovoltaic (FPV) Plant connected to the Spanish electrical network. To analyze the performance, the electrical behaviour of the plant must comply with the grid connection requirements defined by REE in "*P.O. 12.2*", dated October 2018.

From the studies carried out throughout the project, it can be concluded that the FPV plant does not bring any new steady-state voltage disturbance and that the Spanish transmission network is capable to import the generated power by the FPV plant at any time. From the energy quality assessment, it is figured out that the power quality of the PV plant is in alignment with P.O. 12.2 directions and does not introduce abnormal waveforms.

During the dynamic simulations, it was observed that the FPV plant will not pose significant risk to the Spanish transmission network, even though worst case scenarios were considered in many studies.

Therefore, out of these studies it can be concluded that the connection of the proposed 50 MW Floating Photovoltaic Power plant results in full compliance with the Spanish grid code requirements "*Procedimiento de Operación 12.2 - Instalaciones de generación y de demanda: requisitos mínimos de diseño, equipamiento, funcionamiento, puesta en servicio y seguridad*", dated October 2018 and consequently, also complies with the "*Commission Regulation (EU) 2016/631 of 14 April 2016 establishing a network code on requirements for grid connection of generators*".

6.2   Future Works and Challenges

Although several large-scale floating solar energy projects have been developed, still there are certain challenges to deal with in coming years. One of them is the speculation about the costs, which are expected to go down with economies of scale. Another issue is the environmental impact that could be caused in the water. An environmental impact report is specific for each FPV plant, relying on the country's regulations. Finally, regarding the operation of the plant, challenges are set out about the electrical safety and operation and maintenance of the electrical equipment.

On the other hand, another challenge for floatovoltaics is the lack of specific regulations. For the time being, applications and licenses are generated in the same way as on-ground PV. Therefore, in order to encourage the deployment of floating photovoltaic plants, new regulations have to be arranged, including aspects as environmental impact and water rights for the installation of a floating photovoltaic system.

However, floating solar energy opens new opportunities for technologies that are in continuous development. This is the case of bi-facial solar panels. Basically, they have a photovoltaic layer in the back, generating up to 7% more electricity with the reflected rays due to the albedo. Water has one of the most variable albedo coefficients, between approximately 40-70%. Consequently, a floating solar plant composed by bi-facial PV modules, can achieve an energy yield up to 21% higher than a common ground-mounted PV plant.

Another alternative is to combine floatovoltaics with existent pumped-storage hydropower plants. These hybrid systems can become the solution for large-scale energy storage, as the excess solar energy generated will be used to feed the water pumps, pumping the water from the lower reservoir to the higher one [9]. In this way, floating solar capacity will be able to import electricity to the electrical system but also, it will be used to store energy continuously.

Bibliography

[1] Solar Energy Research Institute of Singapore, *Where Sun Meets Water. Floating Solar Market Report.* World Bank Group, 2018. Available: https://www.worldbank.org/en/topic/energy/publication/where-sun-meets-water

[2] S. Ong et al. *Land-use requirements for solar power plants in the united states.* National Renewable Energy Lab.(NREL), Golden, CO (United States). 2013.

[3] Ciel & Terre: The Floating Solar Expert. Available: https://www.ciel-et-terre.net.

[4] Plan Nacional Integrado De Energía Y Clima (PNIEC) 2021-2030. February 2019 Available: https://www.idae.es/informacion-y-publicaciones/plan-nacional-integrado-de-energia-y-clima-pniec-2021-2030.

[5] A. Dizier, Techno-Economic Analysis of Floating PV Solar Power Plants using Active Cooling Technique. KTH School of Industrial Engineering and Management, 2018.

[6] S. Bhattacharjee, Floating Solar Power Plants - A promising technology that needs time to evolve. JAKSON . Published on August 18, 2008. Available at: https://www.jakson.com/blog/floating-solar-power-plants-a-promising-technology-that-requires-time-to-evolve/

[7] J. A. Roca, Conectan la planta fotovoltaica flotante más grande del mundo en

China, 2019. Available: https://elperiodicodelaenergia.com/conectan-la-planta-de-fotovoltaica-flotante-mas-grande-del-mundo-en-china.

[8] I. Kougias et al, *The potential of water infrastructure to accommodate solar PV systems in Mediterranean islands,* vol. 136, pp. 174-182, 2016. DOI: 10.1016/j.solener.2016.07.003.

[9] J. Farfan and C. Breyer, *Combining Floating Solar Photovoltaic Power Plants and Hydropower Reservoirs: A Virtual Battery of Great Global Potential*, vol. 155, pp. 403-411, 2018. DOI: 10.1016/j.egypro.2018.11.038.

[10] JKM315P-72 295-315 Watt Poly Crystalline Module. Jinko Solar. Technical Report. Available: https://www.jinkosolar.com/ftp/EN-JKM315P-72(4BB).pdf.

[11] Wysocki, Joseph J ad Rappaport,Paul, *Effect of temperature on photovoltaic solar energy conversion,* Journal of Applied Physics, vol. 31, (3), pp. 571-578, 1960.

[12] O. Wasynezuk, Dynamic Behavior of a Class of Photovoltaic Power Systems, *IEEE Transactions on Power Apparatus and Systems*, vol. PAS-102, (9), pp. 3031-3037, 1983. . DOI: 10.1109/TPAS.1983.318109.

[13] EDP, Ed., *A Hybrid Hydropower and Floating PV System in Portugal*. International Hydropower Association, 2017. Available at: https://www.hydropower.org/sites/default/files/publications-docs/case_study_-_a_hybrid_hydropower_and_floating_pv_system_in_portugal.pdf

[14] A. Sahu, N. Yadav and K. Sudhakar, Floating photovoltaic power plant: A review. *Renewable and Sustainable Energy Reviews*, vol. 66, pp. 815-824, 2016.

[15] G. K. X. Melvin, *Experimental study of the effect of floating solar panels on reducing evaporation in Singapore reservoirs*, National University of Singapore, 2015.

[16] K. Sudhakar, *SWOT analysis of floating solar plants*, MOJ Solar Photoen Sys, vol. 3, (1), pp. 20-22, 2019.

[17] J. A. Roca, *Las 10 mayores centrales hidroeléctricas de España*, July 13, 2015. Available: https://elperiodicodelaenergia.com/las-10-mayores-centrales-hidroelectricas-de-espana/

[18] Propuesta P.O. 12.2, Instalaciones De Generación Y De Demanda: Requisitos Mínimos De Diseño, Equipamiento, Funcionamiento, Puesta En Servicio Y Seguridad. Red Eléctrica de España (REE), October 2018. Available: https://api.esios.ree.es/documents/449/download?locale=es

[19] Commission Regulation (EU) 2016/631 of 14 April 2016 - Establishing a Network Code on Requirements for Grid Connection of Generators. Available at: https://eur-lex.europa.eu/legal-content/EN/TXT/HTML/?uri=CELEX:32016R0631&from=EN.

[20] R. Iturria, "Nuevo Código de Red Español. ¿La revolución de las renovables?", 2019. Available: https://www.vectorcuatrogroup.com/nuevo-codigo-de-red-espanol-la-revolucion-de-las-renovables/.

[21] IEC TR 61000-3-7: Electromagnetic compatibility (EMC) - Part 3: Limits - Section 7: Assessment of emission limits for fluctuating loads in MV and HV power systems

[22] IEC TR 61000-3-6: Electromagnetic compatibility (EMC) - Part 3: Limits - Section 6: Assessment of emission limits for distorting loads in MV and HV power systems

[23] IEC TR 61000-3-13: Electromagnetic compatibility (EMC) - Part 3: Limits - Section 13: Assessment of emission limits for the connection of unbalanced installations to MV, HV and EHV power systems

[24] WECC Guide for Representation of Photovoltaic Systems In Large-Scale Load

Flow Simulations, WECC Renewable Energy Modeling Task Force, Tech.Rep, 2010.

[25] A. Ellis, M. Behnke and C. Barker, *PV system modeling for grid planning studies*, in 2011 37th IEEE Photovoltaic Specialists Conference, 2011.

[26] Power Electronics. HEMK Inverter Technical Characteristics - PQ Curve

[27] DiSILENT Ibérica. Conexión a Red De Plantas De Energía Renovable Con DigSI-LENT PowerFactory y GridCode 2019. March 2019.

[28] IEEE Std 141-1993: Recommended Practice for Electric Power Distribution for Industrial Plants, pp. 1-768, 1994. . DOI: 10.1109/IEEESTD.1994.121642.

[29] IEEE Std 399-1997: Recommended Practice for Industrial and Commercial Power Systems Analysis, pp. 1-488, 1998. DOI: 10.1109/IEEESTD.1998.88568

[30] IEC 60909-0:2016 - Short-circuit currents in three-phase a.c. systems - Part 0: Calculation of currents, 2006.

[31] Electricity Association. *Planning limits for voltage fluctuations caused by industrial, commercial and domestic equipment in the United Kingdom.* Engineering Recommendation Practice 28, vol. 28, pp. 1989, 1989.

[32] IEC 61400-21-1: Measurement and assessment of power quality characteristics of grid connected wind turbines. 2019.

[33] Power Electronics. Harmonics results report in freesun HEMKH inverters. January 2019

[34] Power Electronics.Flicker results report in freesun HEMKH inverters. January 2019

Appendix A

Technical data of the FPV electrical equipment

The electrical parameters for the medium voltage collector circuits and the overhead transmission line are given in Table A.1.

In Tables A.2 and A.3 the useful technical for modelling the step-up 30/0.66 kV and 132/30 kV, respectively, are presented.

The relevant information extracted from the datasheet of the inverters is included in Table A.4.

For the energy quality studies, it is necessary to know the harmonics current contribution flicker coefficients from the inverters. The harmonic currents have been obtained after several tests performed according to IEC 61000-3-12. The flicker coefficients have been measured at 100 % of the nominal power of the inverter, at inverter start-up and shut-down complying with IEC 61000-4-15. These information is privileged and confidential. Therefore, its content cannot be included without a written authorization of Power Electronics España.

Table A.1: MV and HV cables technical data

Cable ID	I_{max} [A]	$R_{ac}^{20°C}$ [Ω/km]	X_+ [Ω/km]	R_0 [Ω/km]	X_0 [Ω/km]	C_+ [uF/km]
1x95 mm2 2XS2YRAA - 30 kV	292	0.1930	0.1288	0.9650	0.4508	0.17
1x150 mm2 2XS2YRAA - 30 kV	366	0.1240	0.1225	0.7316	0.3675	0.1900
1x240 mm2 2XS2YRAA - 30 kV	475	0.0754	0.1100	0.5504	0.1853	0.2300
LA 280 HAWK - 132 kV	660	0.1190	0.3800	0.6283	1.3000	0.0094

Table A.2: Power Station Transformer electrical data

Step-Up Transformer		
Voltage Ratio	[kV]	30/0.66
Quantity	[ ]	16
Power Rating	[kVA]	3,800
Winding Type	[ ]	2-winding
Cooling Type	ONAN/ONAF	ONAN
Vector Group	[ ]	Dy11
Short-circuit impedance	[%]	6.75
Load loss	[kW]	35
No load loss	[kW]	2.69
Tap changer	[ ]	± 2x2.5%
X/R ratio	[ ]	7.25

Table A.3: Substation Transformer 132/30 kV electrical data

Power Transformer		
Voltage Ratio	[kV]	132/30
Quantity	[ ]	1
Power Rating	[MVA]	60
Winding Type	[ ]	2-winding
Cooling Type	ONAN/ONAF	ONAF
Vector Group	[ ]	YNd11
Short-circuit impedance	[%]	12.5
Copper losses	[kW]	166.6255
No load losses	[kW]	75
Tap changer	[ ]	± 10x1.25%
X/R ratio	[ ]	45

Table A.4: PV Inverter ratings and technical characteristics

Solar PV Inverter		
Inverter Model	[ ]	FS3510K
Quantity	[ ]	16
Rated AC Voltage	[V]	660
Operating Grid Voltage	[V]	660± 10%
Maximum DC Voltage	[V]	1500
Rated Power	[kVA/kW]	3630@40°C 3510@50°C
Frequency	[Hz]	50/60
Power Factor	[ ]	Adjustable

Appendix B

Inverter Parameterization

In this section, the inverter's dynamic model described in Chapter 4 is parameterized. This appendix refers to the inverter controller (Table B.1), PPC (Table B.2) and protections (Table B.3) variables parameterization.

Table B.1: User defined inverter Controller parameterization

Variable	Value	Description
ramp_up_p_out	500	Active power ramp up LVRT recovery [%/s]
PPCon	1	=0 (PCC off), =1 (PCC on)
Pref	1	Inverter active power reference [pu]
Qref	1	Inverter reactive power reference [pu]
Kp_qi	1	Q controller: proportional gain
Ki_qi	10	Q controller: integral gain
Plim	1	Active power limitation [pu]
Qlim_cap	1	Capacitive reactive power limitation [pu]
Qlim_ind	1	Indutive reactive power limitation [pu]
PQ_priority	1	=1 (P priority); =0 (Q priority)
ramp_up_p	100	Active power ramp up [%/s]
ramp_down_p	-100	Active power ramp down [%/s]
ramp_up_q	20000	Reactive power ramp up [%/s]
ramp_down_q	-20000	Reactive power ramp down [%/s]
Tp	0.01	Active current lag time [s]
Tq	0.01	Reactive current lag time[s]
lvrt_th	0.85	LVRT threshold [pu]
hvrt_th	1.2	HVRT threshold [pu]
K_lvrt	2	LVRT K factor
K_hvrt	0.5	HVRT K factor
LVRT_mode	0	=0(Id=0); =1 (Id = Id_{prev})
hyst	0.05	LVRT hysteresis
Tv	0.02	Voltage measurement lag time [s]

Table B.2: User defined Pwer Plant Controller (PPC) parameterization

Variable	Value	Description
Pref_poi	1	POI P reference [pu]
FRon	1	=0 (FR disabled), =1 (FR enabled)
fon	50.2	Positive activation frequency [Hz]
foff	49.8	Negative activation frequency [Hz]
fn	50	Rated frequency [Hz]
K_fr	50	FR slope [/Hz]
Tf	0.01	Frequency measurement lag time [s]
Tpc	0.01	Active power command lag time [s]
PPC_Qcont	1	0 (disabled), 1 (Vpoi), 2 (Qpoi), 3 (PFpoi)
Vref_poi	1	POI voltage reference (PPC_Qcont=1)
Kp_v	10	V poi controller: proportional gain
Ki_v	10	V poi controller: integral gain
Qref_poi	1	POI reactive power reference (PPC_Qcont=2)
Kp_q	0.1	Qpoi controller: proportional gain
Ki_q	2	Qpoi controller: integral gain
PFref_poi	0	POI power factor reference (PPC_Qcont=3)
vsat	0.9	PPC saturation threshold
Tv	0.01	POI voltage measurement lag time [s]
Tq	0.01	POI reactive power measurement lag time [s]
Tqc	0.01	POI reactive power command lag time [s]

Table B.3: Voltage and Frequency Protections parameterization

Variable	Value	Description
PRon	1	1 (Prot.Enabled), 0 (Prot. Disabled)
v_hf	1.2	Voltage High-Fast Limit [pu]
v_hs	1.15	Voltage High-Slow Limit [pu]
v_ls	0.85	Voltage Low-Slow Limit [pu]
v_lf	0	Voltage Low-Fast Limit [pu]
Tv_hf	0.05	Delay for Voltage High-Fast Limit [s]
Tv_hs	1	Delay for Voltage High-Slow Limit [s]
Tv_ls	1.35	Delay for Voltage Low-Slow Limit [s]
Tv_lf	0.15	Delay for Voltage Low-Fast Limit [s]
f_hf	1.03	Frequency High-Fast Limit [pu]
f_hs	1.02	Frequency High-Slow Limit [pu]
f_ls	0.97	Frequency Low-Slow Limit [pu]
f_lf	0.95	Frequency Low-Fast Limit [pu]
Tf_hf	0	Delay for Frequency High-Fast Limit [s]
Tf_hs	1800	Delay for Frequency High-Slow Limit [s]
Tf_ls	1800	Delay for Frequency Low-Slow Limit [s]
Tf_lf	0	Delay for Frequency Low-Fast Limit [s]

Appendix C

FPV plant single line diagram

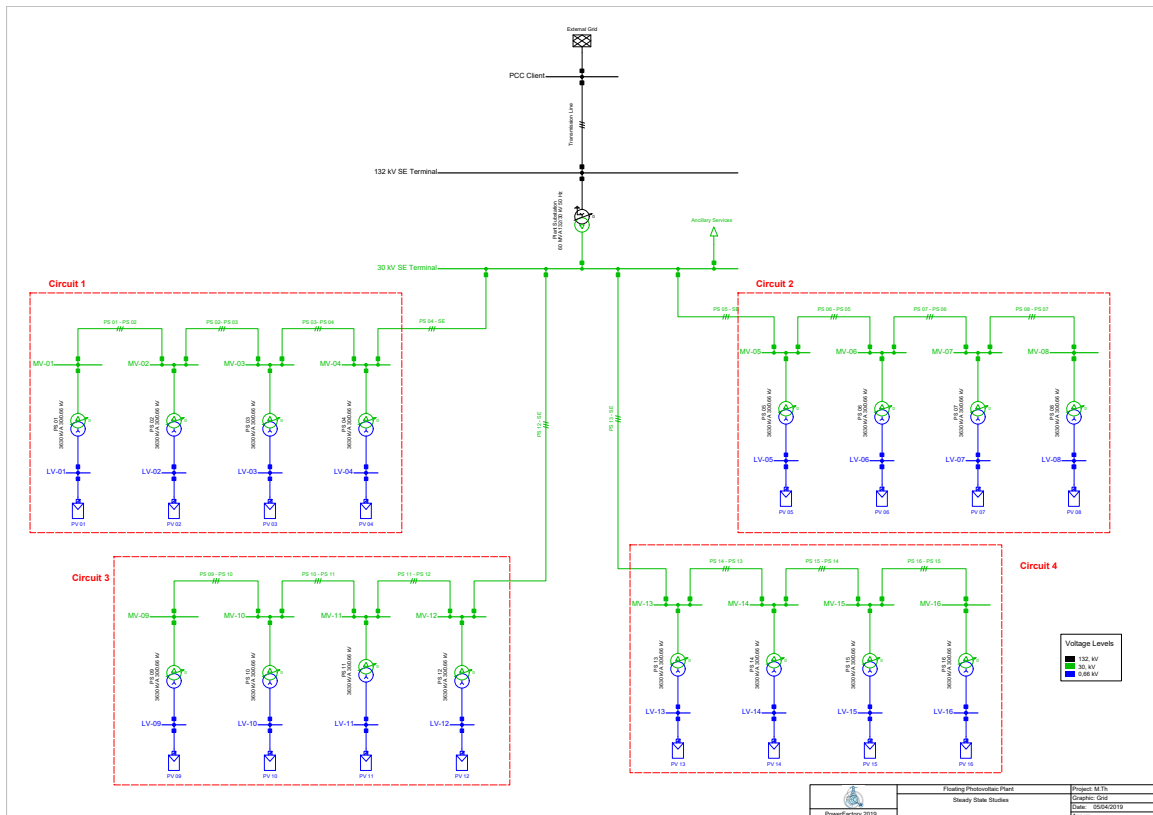This appendix shows a detailed single line diagram of the floating PV plant modelled in PowerFactory.

Figure C-1: Floating Photovoltaic Plant detailed single line diagram